

11

The extraction of melt from crustal protoliths and the flow behavior of partially molten crustal rocks: an experimental perspective

E. H. RUTTER AND J. MECKLENBURGH

11.1 Introduction

Other chapters in this book deal with melting reactions and the fertility of crustal protoliths (Chapter 9), patterning of melt-depleted lower crustal rocks (Chapter 10) and the ascent and emplacement of magma to form plutons (Chapter 13). In this chapter we are concerned with physical processes in the source region – where melt-producing reactions lead to a rock permeated with viscous fluid – the ways in which the strength of this rock is affected by a developing melt fraction, the mechanisms by which the fluid collects into bodies that may ascend to higher crustal levels, and the mechanical properties of partially molten crustal rocks in those circumstances where melt is unable to escape.

The principal forces to which the partially molten system responds are: (1) gravitationally induced forces, due primarily to the density difference between the melt phase and the matrix of solid crystals; (2) tectonic forces, that produce either elastic or permanent distortion of the rock mass, and (3) surface tension forces that arise between melt and the crystalline matrix. The most important physical properties of the components of the system are: (1) the viscosity of the melt phase, which varies principally with temperature and content of dissolved water or other volatiles; (2) the rheological properties of the crystalline framework of grains (whereas the melt fraction is sufficiently small that they remain inter-connected), and (3) the permeability of the crystalline framework to the flow of the melt phase through it. The permeability may be due either to the inter-granular network of connected pores, and/or to the development of a network of variously connected cracks or veinlets, or to compositional layering developed prior to melting or as a result of the melting process itself. Thus, the melt distribution may be heterogeneous on a number of length scales. We will assume that porosity may be equated to the melt fraction. This is equivalent to assuming that the solid matrix is fully saturated with melt.

The mechanical behavior of a porous solid saturated with fluid at low temperatures is treated by soil mechanics. Although the fluid is a viscous melt at high temperature, we will argue that useful parallels may be drawn between soil mechanics and the behavior of partially molten rocks. However, there are important differences. The solid framework of a weak rock or soil at low temperature shows little or no dependence of its strength on elapsed time or rate of deformation. However, time-dependent effects do arise from the viscous flow of water into or out of the pore spaces, with consequent effects on porosity and mechanical strength. These considerations apply also to partially molten rocks, but in addition partially molten rocks may display a range of deformation mechanisms that are strongly rate-dependent in their own right, because the solid framework of crystalline grains is at high temperature. Thus, the strength of the rock will decrease as deformation rate decreases. Whereas the compaction of a soil takes place almost exclusively by relative motion of the grains with respect to each other, thereby changing the packing density, crystalline rocks at high temperature may compact by a number of mechanisms. They may fracture at the grain scale, or individual crystals may become internally plastically deformed by dislocation motion. Distortion and compaction of the grain framework also may take place by diffusive mass transfer through the melt by dissolution from more highly stressed grain contacts and concomitant crystallization of the same or new phases in the melt-filled spaces.

Much of what we know about the flow behavior of partially molten rocks comes from high pressure/temperature deformation experiments on small samples of natural or synthetic materials. Experimental data may be applied to models of natural processes of deformation and melt extraction, in order to estimate the rates of those processes, and to obtain insights that might be tested against field observations. It is important always to remain aware of the fact that processes in partially molten rocks in nature take place on a range of length scales, from the granular to kilometric. Experimental studies only provide information about processes on the grain scale, or where heterogeneities of stress, mineralogy, or melt distribution may develop over the range of the specimen length. The link between experiment and nature must be made via mathematical modeling or, where appropriate, analog modeling.

For some physical mechanisms of flow of partially molten rocks, it is possible to derive flow and compaction/melt-extraction laws entirely from physical first principles, although one aims to test such laws against the results of experiments. A major aim of this chapter is to summarize the kind of information that has been obtained from such mechanical experiments. We will then discuss the theoretical framework for the interpretation of the results of experiments, and the ways in which these ideas may be applied to natural

deformation of partially molten crustal rocks and the extraction of granitoid melts as the first step in pluton formation.

11.2 Deformation mechanisms

Deformation of partially molten rocks in which the matrix of solid grains forms a mechanically interconnected framework is expected to involve distortion of the framework by one or some combination of mechanisms (1)–(3) below (also Fig. 11.1). Whenever deformation involves a succession of physical

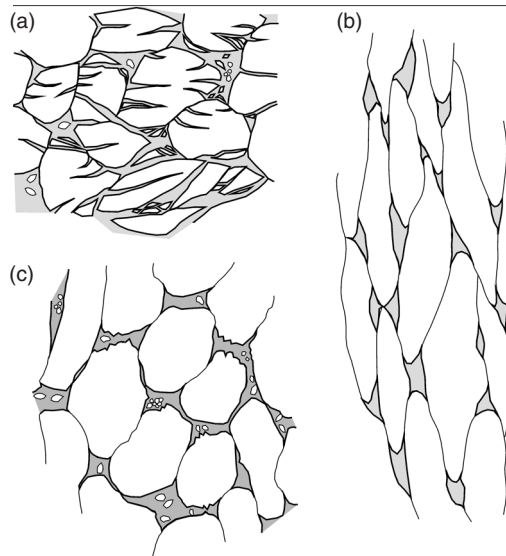


Fig. 11.1. Sketches to illustrate the main features at the grain scale of the deformation mechanisms likely to be important in partially molten rocks. In each case, the compression direction is horizontal, strain path is irrotational, grains are white and the melt phase is shaded gray. (a) Cataclastic-frictional deformation, characterized by grain fragmentation without internal distortion, and frictional sliding between fragments. There is a strong preferred orientation of cracks parallel to the maximum compressive stress direction. (b) Intracrystalline deformation of the solid phases, resulting in a shape-preferred orientation of grains, and probably also a crystallographic-preferred orientation. (c) Granular flow. The fundamental strain accumulation process is slippage of grains with respect to one another. Locking asperities may be removed to allow slippage either by diffusive transfer through the melt phase, leading to formation of overgrowths on grains or neocrystallization in the melt, or by fracture of locking points if grains have become sintered together. If the grains tend originally to tabular habits, a shape-preferred orientation of the grains would be expected. (b) and (c) are likely to be more important than (a) in nature.

processes, the slowest one is expected to control the overall rate. Rosenberg (2001) provides a comparative review of deformation mechanisms in naturally and experimentally deformed partially molten granitic rocks.

- (0) Fracturing of the framework of grains, with frictional sliding of the fragments. The crystal structure of the fragments remains undistorted, but the rock mass may change shape, and may be accompanied by volumetric dilatation or compaction. Compaction may be brought about by closer packing of fragments, or concentrating small, spalled fragments into melt-filled spaces between larger grains. Alternatively, frictional sliding of whole grains may occur without fracturing. Because the resistance to deformation arises principally through resistance to fracture and frictional forces, the strength is expected to be dependent strongly on the difference between confining pressure and melt pressure (i.e., effective pressure) but only weakly sensitive to large changes in deformation rate or temperature change. Variations in effective pressure may arise through dilatancy or compaction; hence, rate dependencies on strength may arise (at least on the time scale of experiments) according to the resistance to viscous flow of the melt between grains. All experimental studies of deformation of partially molten granitic rocks at low to moderate confining pressures (<500 MPa) and high strain rates ($\dot{\epsilon} > 10^{-6} \text{ s}^{-1}$) have induced this type of deformation (e.g., Arzi, 1978; van der Molen & Paterson, 1979; Paquet & François, 1980; Paquet *et al.*, 1981; Rutter & Neumann, 1995).
- (1) Intracrystalline plastic deformation of the constituent grains of the framework. Individual crystals distort internally, leading to shear deformation of the rock mass and compaction if the melt phase may be expelled (drained conditions)

$$\dot{\epsilon} = C\sigma^n \exp(-H/RT), \quad (11.1)$$

in which $\dot{\epsilon}$ strain rate, C is an empirical constant, σ is the flow stress, n is an empirical constant that defines the strain rate sensitivity to stress, $d \log \dot{\epsilon} / d \log \sigma$ (commonly about 4, so that strength is more sensitive to flow rate than in (1) above), T is temperature in K, R is the gas constant, and H is the heat of activation (activation enthalpy) for flow. H effectively defines the temperature sensitivity of the flow rate (at constant stress), according to

$$H = -R \frac{d \log_e \dot{\epsilon}}{dT^{-1}}. \quad (11.2)$$

Intracrystalline plastic processes are commonly characterized by $H > 2 \times 10^5 \text{ kJ mol}^{-1}$, which means that strain rate is relatively sensitive to temperature change at constant stress. Dell'Angelo *et al.* (1987), Dell'Angelo and Tullis (1988) and Gleason *et al.* (1999) have shown that, during deformation of partially molten granitic rocks at 1.5 GPa confining pressure in solid-media apparatus, the quartz grains in the matrix flow by intracrystalline plasticity.

- (2) Granular flow with various accommodation mechanisms. Granular flow is comparable geometrically to the process of frictional sliding of unfractured grains

forming a porous aggregate (cf. the flow of cohesionless sand), except that the rate of the process is determined by the kinetics of removal of the asperities or sticking points at grain contacts.

Paterson (2001) considers in detail several processes for the accommodation of the intergranular displacements (accommodation processes). For the case where congruent pressure-melting may occur at highly stressed contacts between grains (e.g., water-ice), the deformation may be rate-limited by the viscous flow of new melt along intergranular contacts to lower-pressure regions. For the case of incongruent pressure-melting or transfer of “dissolved” components of the solid phase in a supposed intergranular melt phase, the rate may be controlled either by the rate of diffusion of the grain component(s) in the melt (diffusion control) or by interface kinetics (reaction control), the latter meaning the rate of detachment of solid phase components at the source (stressed grain contact region) or reattachment at the sink (reprecipitation site).

Hirth and Kohlstedt (1995b) described this process in olivine aggregates pervaded by basaltic melt. However, from transmission electron microscopy (TEM) they reported no wetting of stressed grain interfaces by melt, and concluded that the acceleration of flow (relative to melt free aggregates of olivine of the same grain size) was due to short-circuit diffusive transfer across melt filled pores to the reprecipitation site, with solid state diffusive transfer of material in the stressed interfaces to the edge of the melt filled pores.

These types of process are expected to follow a flow law of the form

$$\dot{\epsilon} = C\sigma \exp(-H/RT)d^{-m}, \quad (11.3)$$

in which grain size, d , is introduced, raised to a power, m , which might take a value ideally of about 3. The length scale introduced by the grain size is assumed to represent the distance between sources and sinks for diffused matter. The expected linear relationship between strain rate and stress means that it should be favored over other, non-linear processes by relatively low strain rates and/or low stresses. Therefore, it should be least amenable to experimental study, because care would have to be taken to avoid operation of the other processes that are more easily activated at experimentally accessible strain rates (Fig. 11.2). The combination of high temperatures with low strain rates for the deformation of partially molten rocks in nature should favor a diffusion accommodated granular flow process, and small grain sizes should make it even more competitive relative to fracture or intracrystalline plasticity (Dell’Angelo *et al.*, 1987).

The effective operation of diffusion accommodated granular flow depends on whether melt films may exist or be generated in stressed grain boundaries. This issue is discussed further below, but a competing process may be sintering

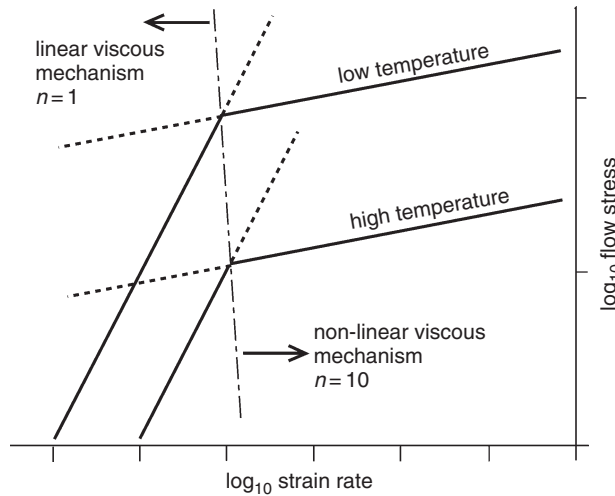


Fig. 11.2. Schematic illustration of how a high numerical value of the stress exponent in a constitutive flow law may make it difficult experimentally to access deformation mechanisms characterized by linear viscosity. Increasing stress at high strain rates preferentially accesses the more nonlinear process. Even increasing temperature may not always help if the boundary between the two processes is not very strain rate-sensitive (as here). The linear viscous process can be accessed only by substantially lowering the strain rate. Provided the linear viscous process is diffusion-controlled, it may alternatively be favored by enhancing kinetic factors such as adding water to increase diffusivity or by reducing grain size.

and neck growth at grain contacts. This process is driven by the surface energy differences between liquid and solid phases that attempt to remove small curvature interfaces between solids and liquid. Transported and redeposited solid to form “necks” may be derived from the walls of pore spaces or by diffusive transfer along melt-bearing interfaces, or both. The process reduces intergranular contact stresses, inhibiting intergranular diffusion creep and causing hardening. Granular flow may still take place, but may become dependent on the failure of the sintered contacts by fracture rather than by purely diffusive processes. Although little is known of high-temperature fracture processes, especially in the presence of a melt phase, we may anticipate that the geometric stress intensification that occurs at crack tips will require a non-linear relation between applied stress and overall strain rate. Thus, a process like this may supervene in high strain rate experiments which otherwise might be expected to show diffusive transfer creep (Fig. 11.2).

In each of the above processes, the relative movement of framework grains requires some viscous flow of the melt phase. At high-melt viscosities,

high-applied stresses, and fine grain sizes, it is possible that the overall rate of deformation might be controlled by the flow of the melt phase, as pore (= melt) spaces distort, dilate, or compact. Whereas this may be important in studies at some experimental strain rates and grain sizes, it is unlikely to be so at geological rates and grain sizes.

11.3 Experimental studies of partially molten rocks

11.3.1 Experimental methods

Rather few (on the order of ten to twenty) experimental studies of the mechanical behavior of partially molten crustal rocks under high pressure have been carried out. A similar number of experimental studies has been made of partially molten ultrabasic rocks, containing basaltic melts. Despite the fact that basaltic melts are generally much less viscous than granitoid melts, these studies also have some relevance for understanding the behavior of crustal rocks during partial melting.

Experimentalists have tended to approach the behavior of fully or partially molten rocks from either end of a melt fraction spectrum. Those who are concerned with the viscosity of melt phases and the effect of adding increasing volumes of solid-phase grains must employ methods such as falling sphere or rotating cylinder viscometry. In either case, a container must be used to support the melt, especially if viscosity is low. At the other end of the spectrum are those who are concerned primarily with the effect of a small volume fraction of melt on rheological behavior. Here, axisymmetric compression of cylindrical samples or various direct shear configurations may be used. Where the melt phase is very viscous, this approach may be used even with melt fractions in excess of 40%, but owing to the tendency to approach the problem from either the 100% solid or 100% liquid ends of the spectrum, relatively few data are available for behavior in the middle of the range.

For experiments carried out on “relatively solid” samples, cylindrical test pieces are used, up to 1 cm diameter and 2 cm in length. They may be samples cored from natural rocks or fabricated by hot isostatic pressing of powders. In the latter case, a refractory solid phase is mixed with a proportion of glass of appropriate composition, which melts at the temperature of the experiment. A small percentage of water may be added to the sample, or it may be tested “dry.” If hydrous phases (e.g., micas or amphiboles) are present initially in the sample, they may break down at test temperatures to yield a melt into which the water has dissolved. Samples must generally be sealed inside a ductile metal sleeve, to separate the confining pressure medium from the sample, and to prevent loss of melt (and water if added to the experiment).

Two types of testing machine have been used for deformation experiments on partially molten rocks. These methodologies are reviewed by Tullis and Tullis (1986), Paterson (1990) and Green and Borch (1990). In solid-medium machines, a ductile solid is used to apply the confining pressure. A disadvantage of this approach is that the confining medium has some intrinsic shear strength, and it may not be possible to measure accurately the low strengths of the partially molten rock sample if melt fractions are large. This disadvantage has been overcome to some degree through the use of confining media (e.g., salts or glasses) that melt around the specimen under the temperature and pressure conditions of the experiment. In these types of apparatus, high confining pressures (>1 GPa) may be applied to the specimen. In gas medium machines, an inert gas such as argon is used to apply the confining pressure. Such machines have high resolution of load measurement, but are normally used only to confining pressures of about 500 MPa. Even with this approach, it is difficult to obtain reliable strength data below about 15 MPa differential stress, as the load supported by the ductile metal jacket around the sample begins to be a significant fraction of the load supported by the sample.

In most studies of partially molten rocks, the specimen has been totally sealed, so neither melt nor vapor phase may be lost from the sample, in which case the sample is said to be *undrained*. This means that deformation is constrained to occur under constant volume conditions, once any compaction of initial voids has taken place, even though melt may move from one place to another within the sample. Local variations in melt pressure may be induced during an experiment if the dominant deformation mechanism permits elastic intergranular dilatation. However, if the shear stresses involved in the flow are much less than the confining pressure, pressure fluctuations in the melt will be only small fractions of the confining pressure. During undrained deformation, therefore, there will be almost zero effective confining pressure (applied confining pressure minus pore fluid (melt) pressure) on the sample, and any strengthening effect of the total confining pressure will be near absent. At smaller melt fractions, when the shear strength of the sample may become commensurate with the confining pressure, any dilatancy that occurs may cause a substantial drop in pore pressure and a corresponding rise in effective pressure, which will cause strengthening (Renner *et al.*, 2000). In most deformation experiments on partially molten granitic systems, an equilibrium melt fraction has not been attained during the experiment. The continuous creation of melt will tend to offset dilatancy hardening effects that might otherwise arise, but this factor in the interpretation of the results of deformation experiments has not yet been subjected to systematic study.

It is possible to configure the sample so that it is effectively *drained*. In the case of rocks deformed with water as the pore fluid, this condition would be attained by connecting the sample void spaces to a pore fluid pressure system via a hollow loading piston. In this case, the solid framework of the sample is free to compact or dilate, according to the active deformation mechanism. Pore fluid flows into or out of the sample accordingly, such that pore pressure is maintained constant at a value less than the confining pressure, and any desired effective pressure condition may be imposed. A fully drained (melt pressure = 0) condition may be brought about in a partially molten rock by draining excess melt into a porous but strong solid “sink” at one end of the sample, ensuring that there is sufficient pore space available to accommodate more than the total amount of melt produced (Rutter & Neumann, 1995). Future studies of deformation of partially molten rocks will require drained experiments with independent control of the melt pressure, for only in this way may the kinetics of compaction of the solid framework be studied in a controlled way, with concomitant expulsion of the melt phase (Viskopic *et al.*, 2001; Renner *et al.*, 2003).

11.3.2 Experimental studies on partially molten granitic and related rocks

Some experimental studies on partially molten granitic rocks have used natural rocks deformed in gas-confining medium apparatus at moderate confining pressures (~300 MPa) (e.g., Arzi, 1978; van der Molen & Paterson, 1979; Paquet & François, 1980; Paquet *et al.*, 1981; Auer *et al.*, 1981; Rutter & Neumann, 1995). In all of these studies, deformation of the matrix of solid grains, at least at high strain rates, was by some combination of grain fracturing and sliding between grains or fragments, with some possible but unknown amount of strain by diffusive mass transfer creep. With the exception of a small number of the experiments of Rutter and Neumann (1995), all of these experiments were undrained. Thus, in these experiments, effective confining pressures were not sufficiently high to inhibit fracture, nor were mean pressures on the solid phases high enough to favor intracrystalline plastic flow.

Mechanical data from high-pressure (solid medium, 1500 MPa confining pressure at 900 °C) experiments have been reported for natural granitoid rocks by Dell’Angelo and Tullis (1988) and Dell’Angelo *et al.* (1987). Only in such high-pressure experiments has dislocation creep been described as the mechanism for the deformation of the matrix of solid grains, although (principally microstructural) evidence was presented for a transition to diffusion creep at low stresses, provided the melt fraction was above a certain minimum amount. Unconfined creep experiments have been reported for fine-grained, partially molten synthetic laboradorite polycrystals with up to 12 vol. % melt (Dimanov

et al., 1988), and Lejeune and Richet (1995) described axisymmetric creep experiments to define the rheology of viscous melts of aluminous enstatite and lithium disilicate with various crystallite volume fractions from 0 up to 60%.

The amount of melt in experimental studies on granitic aggregates has been controlled either by the addition of different amounts of water (Arzi, 1978; van der Molen & Paterson, 1979; Dell'Angelo *et al.*, 1987; Dell'Angelo & Tullis, 1988) or by temperature, according to the water released from phyllosilicate mineral breakdown reactions (Paquet & François, 1980; Paquet *et al.*, 1981; Rutter & Neumann, 1995). These effects must be borne in mind when evaluating the results of experiments involving a range of melt fractions. In contrast to previous work on granites, the melt fraction in experiments on partially molten olivine rocks could be held constant over a range of temperatures because it was produced by the addition of a measured amount of basalt glass to the olivine aggregate (e.g., Hirth & Kohlstedt, 1995a,b).

It is either difficult or impossible to maintain constant viscosity of the melt phase through a series of experiments with different melt fractions. Either the melt viscosity decreases at constant temperature with increasing water content, or at constant water content the viscosity decreases with increasing temperature (Fig. 11.3). However, the range of melt viscosities encountered as water

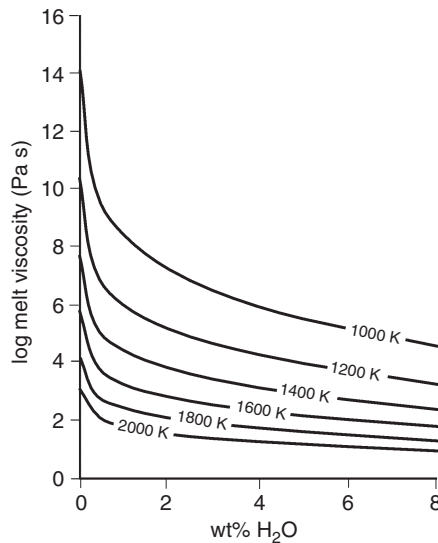


Fig. 11.3. Relationship between temperature, T , water content and melt viscosity, η , for haplogranitic melts according to the fit of Hess and Dingwell (1996) of the form $\log \eta = a + b/(T - c)$, where a , b , and c are functions of water content. Viscosity is particularly sensitive to small variations in water content at water contents less than 1 wt. %.

content is varied is typically much greater than the effect of large variations of temperature. Paradoxically, the viscosity of the melt produced in samples with no water added may increase with increasing temperature. This happens when hydrous minerals present (such as biotite) and any free water are consumed first by the fluid-present melting reactions and then by the fluid-absent incongruent melting reactions. Thus, the water content of the melt will rise initially but then decrease with progressive melting after all the hydrous phases are used up. Fluid-absent dehydration melting of a biotite gneiss due to a melting reaction involving biotite is likely to produce about 15 vol.% melt. Thus, the water content of the melt will increase up to this point and the melt will display low viscosity. Further melting with increasing temperature but no further water added causes viscosity to rise, owing to the strong effect of water on viscosity relative to temperature.

13.3.3 Strength of partially molten granitic rocks at laboratory strain rates

The experimental data of Rutter and Neumann (1995) for Westerly granite at 250 MPa total confining pressure and under undrained conditions show that, at constant water content, increasing temperature leads to a dramatic decrease in strength (Fig. 11.4) which is due to some combination of the way in which

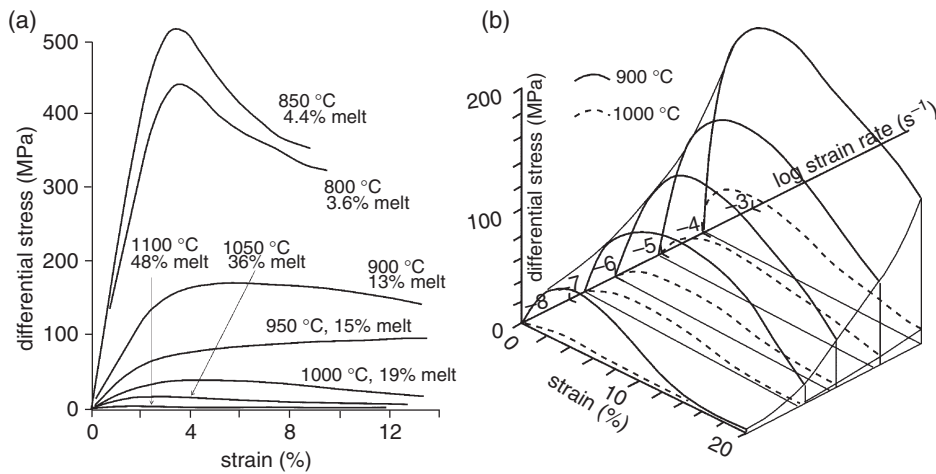


Fig. 11.4. Experimental data on the mechanical properties of partially molten Westerly granite (Rutter and Neumann, 1995) to illustrate the effects of: (a) melt fraction, temperature, and (b) strain rate on strength. Increasing melt fraction through 48% results in a very large (500-fold) decrease in strength and increase in macroscopic ductility. A 10^4 -fold decrease in strain rate reduces strength 5-fold.

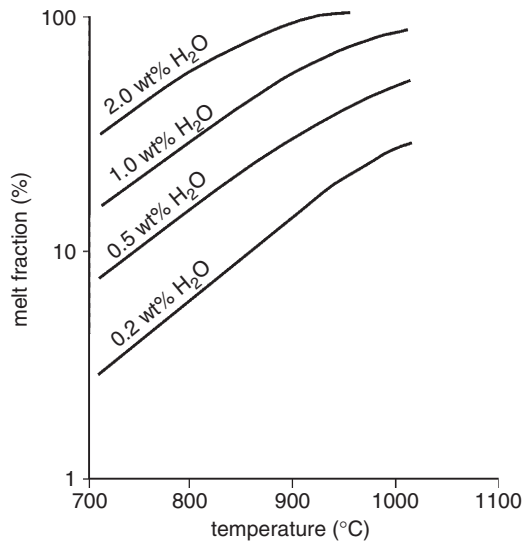


Fig. 11.5. Calculated melt fractions versus temperature for different water contents for a fertile quartzofeldspathic protolith at 500 MPa melt pressure (after Clemens & Vielzeuf, 1987).

temperature reduces the strength of the solid matrix, increases the melt fraction, and decreases the viscosity of the melt. At 850 °C, with 4.4 vol.% melt, the rock supports a differential stress of 500 MPa, but by 1100 °C, with 48 vol.% melt the strength has dropped 500-fold. These melt fractions are only about 60% of the expected equilibrium melt fractions for the temperatures concerned (Clemens & Vielzeuf, 1987; Fig. 11.5), owing to the relatively large grain size of the samples used, the high viscosity of the melt (at a maximum 0.3 wt.% water) and the sluggishness of the melting reactions. Melt fraction, rather than temperature, seems to be the most important control on strength at high strain rates. Up to about 10 vol.% melt, failure involves localization of a cataclastic fault, but at higher melt-fractions the rock flows in a macroscopically wholly ductile manner.

The strength of partially molten granite also decreases with decreasing strain rate (experiments of van der Molen & Paterson (1979) on Delegate aplite, and those of Rutter & Neumann (1995) on Westerly granite). For Westerly granite, the experimental data are described (over the experimentally accessible range) by

$$\dot{\epsilon} = 10^{-5.3} \sigma^{2.9} \exp(-510 \times 10^3/RT). \quad (11.4)$$

This “flow law” is no more than a fit to experimental data, and will not tolerate much extrapolation outside its range. This is because of variable

proportions of cataclasis and granular flow-accommodated deformation across that range, and the melt fraction and melt viscosity varied with temperature. These factors are also included in the apparent activation enthalpy for flow. Nevertheless, extrapolation is likely to lead to conservatively high values for strength at low strain rates. Hence, there is a clear implication that partially molten granite with 10–15 vol.% melt at 800–900 °C, will support a flow stress of less than 1 MPa at a strain rate of $\sim 10^{-11} \text{ s}^{-1}$, a rather fast strain rate by geological standards. In contrast, we would expect about 20 MPa to be required for the intracrystalline plastic flow of quartz at the same conditions (e.g., Luan & Paterson, 1992). Based on available experimental data, only at lower melt fractions and at lower temperatures (about 700 °C) would we expect deformation of partially molten granitic rocks to be strong enough to activate intracrystalline plastic flow of the solid phases. Otherwise, migmatitic crustal rocks should be extremely weak, probably even weaker than suggested above if we invoke diffusion-accommodated granular flow.

11.3.4 Diffusion-accommodated granular flow

Given that we might infer diffusion-accommodated granular flow to be potentially the most important flow process in partially molten granitic rocks, how may it be investigated? Of all deformation mechanisms, diffusion-accommodated flow is the only one that potentially allows the form of the constitutive flow law to be predicted from theoretical considerations, provided the geometric aspects of the rate controlling process may be adequately described. It is also possible to devise experimental approaches dedicated to the isolation of this process.

Theoretical studies

Rutter (1997) and Paterson (2001) have attempted to erect simple models for granular flow. Both are based on the earlier model of Paterson (1995) for granular flow of a water-saturated aggregate. Both model variants predict similar results at the order of magnitude level. The only difference between them is that Rutter (1997) predicts deformation rate $\propto V$ where V is the molar volume of the diffusing component of the solid phase, whereas Paterson (2001) predicts deformation rate $\propto V^2 c'$, in which c' is the concentration of diffusing component in the melt. These differences are due to the fact that, in the former case, the apparent activation enthalpy for creep contains an extra term to account for the energy of formation of a diffusible point defect in the melt phase by thermal fluctuations.

The approach allows the distortional and compactive (or dilatational) components of strain rate to be described separately, and for both undrained (constant total volume except for elastic distortions that allow pore pressure variations – no gain or loss of pore fluid) and drained behavior (compaction with fluid loss allowed). The results depend on the type of stress state imposed, but since we are initially interested in testing such models against the results of axisymmetric compression tests, it is appropriate to assume principal stresses follow $\sigma_1 > \sigma_2 = \sigma_3$. Thus, the deformation may be described by the rate of axisymmetric shortening $\dot{\epsilon}_1$ and the volumetric strain rate $\dot{\phi}$, which is a measure of the rate of flow of melt into or out of the pore spaces (neglecting any elastic volume changes in the solid and assuming no progressive melting). Paterson (2001) investigates three possible rate controlling mechanisms: (1) by viscous flow of melt; (2) by diffusive transfer of dissolved components of the solid phases away from locking points between grains, and (3) control by the kinetics of the dissolution or reprecipitation reactions. Paterson argues that diffusive transfer control is likely to be the most important under geological conditions.

For the open (drained) system, Rutter (1997) predicts

$$\dot{\epsilon}_1 = \frac{C_1 C_2 C_3 V D \phi^r [3(\sigma_1 - \sigma_2) + (\sigma_3 - p)]}{RTd^2}, \quad (11.5)$$

and

$$\dot{\phi} = \frac{C'_1 C'_2 C'_3 V D \phi^r [(\sigma_1 - \sigma_3) + 3(\sigma_3 - p)]}{3RTd^2}, \quad (11.6)$$

in which p is melt pressure, T is temperature in K, d is grain size, and exponent r is taken to be 2 (based on Archie's law, that relates diffusive transport rate through pore fluids to porosity). Constants C_1 , C_2 , and C_3 (and their corresponding primed values) describe the geometry of the grain interfaces and their packing. The primed values are given by

$$C'_1 \approx 6; C'_2 \approx 1/4 \left[\pi / (1 - 0.4\phi^{2/3}) \right]^{1/2}; C'_3 \approx (1 - 0.4\phi^{2/3})^{-1}. \quad (11.7)$$

We will assume $C_1 C_2 C_3 \approx C'_1 C'_2 C'_3$. The term in square brackets in Eq.(11.6) is the effective mean pressure. Renner *et al.* (2003) showed experimentally that compaction rate is proportional to effective mean pressure in melt-saturated peridotite.

In the formulations of Eqs. (11.5) and (11.6), the effective thickness of an assumed melt layer existing in stressed grain boundaries does not appear explicitly because a lower effective bulk diffusivity is assumed, proportional

to ϕ^r . Although depending on the melt film thickness and grain packing geometry, this approximation is likely to lead to some overestimation of deformation rate by Eqs. (11.5) and (11.6) that can be resolved only by experiments. The question of whether stressed intergranular melt films may generally exist is debated widely. In their experimental samples, Hirth and Kohlstedt (1995b) could not detect basaltic melt films between stressed olivine grains (see also Hiraga *et al.*, 2002). On the other hand, melt-assisted sintering is a widely employed technique in the fabrication of several industrial ceramics (e.g., Mortensen, 1997), in which stable, siliceous intergranular melt phases of the order of 1 nm equilibrium thickness have been detected by high resolution TEM (e.g., Clarke, 1987). Drury and Fitzgerald (1996) inferred from TEM observations the existence of nanoscale silicic melt films in polymineralic ultrabasic rocks. The equilibrium thickness of such melt films is expected to depend strongly on the mineralogy of adjacent grains and their orientation relationships when they are mineralogically identical.

The stress components $(\sigma_1 - \sigma_3)$ and $(\sigma_3 - p)$ may be understood primarily as those driving distortion of the aggregate in the absence of effective pressure, and melt flow in the absence of stress difference, respectively. Thus, in the drained condition, $(\sigma_1 - \sigma_3)$ only increases slightly the rate of melt extraction relative to $3(\sigma_3 - p)$ (i.e., differential stress has a small effect on melt flow kinetics unless $(\sigma_1 - \sigma_3) \gg \sigma_3 (\sigma_3 - p)$). Given the weakness of partially molten granite, this seems unlikely. However, the real role of deformation in enhancing melt flow depends on the distance over which pressure gradients are developed (i.e., the gradients $d(\sigma_1 - \sigma_3)/dz$ and $d(\sigma_3 - p)/dz$, as discussed further below).

In order to evaluate these models, it is necessary to know how the melt fraction ϕ and the diffusion coefficient D vary with temperature and water content. These must be constrained by fits to empirical data, which may be rather approximate, especially for extrapolation outside the range of the experiments. Chekmir and Epel'baum (1991) report the following relation between viscosity (η , in Pascals per second) and diffusivity (D of SiO_2 in granitic melts, in square meters per second)

$$\log_{10} D = -0.58 \log_{10} \eta - 10.633. \quad (11.8)$$

The viscosity of dry, silica-rich melts is very high ($\sim 10^8 \text{ Pa s}^{-1}$ at 1100°C , Fig. 11.3) compared to that of basalt melt ($\sim 1 \text{ Pa s}$) at the same temperature. This is because silica-rich melts are highly polymerized, with few cations to break up the polymerization. The structured nature of silica-rich melts is reflected in the small value of entropy change on melting. On the other hand, total saturation of the melt with water may reduce the viscosity by up to 6 orders of magnitude at the lower temperatures in the suprasolidus range, by breaking up silica

tetrahedra, and even 1 wt.% water may reduce viscosity by 3 orders of magnitude (Persikov *et al.*, 1990).

Over the temperature and viscosity ranges relevant for viscous flow of melts in the earth, viscosity may be significantly non-Arrhenian; the apparent activation enthalpy for viscous flow may vary significantly with temperature. For haplogranitic melts, Hess and Dingwell (1996) propose an empirical description of the form

$$\log_{10} \eta = a + b/(T - c), \quad (11.9)$$

where a , b , and c are functions of water content (ψ wt.%) and T is in K. Through fitting to a wide range of experimental data they obtained $a = -3.545 + 0.833 \log_e(\psi)$, $b = 9601 - 2368 \log_e(\psi)$ and $c = 196 + 32.25 \log_e(\psi)$. The predictions of this model (± 0.46 log units of viscosity) are shown in Fig. 11.3.

From the data of Clemens and Vielzeuf (1987), melt fraction may be related to water content and temperature T_c (in Celsius) for a “fertile” protolith (Fig. 11.5):

$$\phi = 10^{-3.68\psi^{0.9}} \exp(0.00875T_c). \quad (11.10)$$

Using Eqs. (11.8) and (11.9), the predictions of Eq. (11.5) are shown graphically in Fig. 11.6 for a grain size of 1 mm and for a range of melt fractions – although in nature the actual melt fraction for a given composition would be fixed by water content and temperature (e.g., by an expression like Eq. (11.10)). The relative sensitivities of strain rate to melt percentage, water content (affecting melt viscosity) and temperature may be seen, for a fixed flow stress of 1 MPa. Strain rates for intracrystalline plastic flow are also shown, calculated from the “average quartzite” model of Paterson and Luan (1990). Intracrystalline plasticity is expected only to become competitive with diffusion-accommodated granular flow at relatively low temperatures in the supra-solidus regime, low water contents and low melt percentages, if grain size is increased and/or stress is increased.

Experimental studies focusing on granular flow processes

To test the above theoretical flow laws against experiment it is necessary to use synthetic samples for mineralogical simplicity, to control the grain size of the solid phase and ideally to control the melt fraction independently of temperature and water content. This type of approach has been employed successfully in studies of olivine rocks with small amounts of Mid-Ocean Ridge Basalt (MORB) melt (e.g., Hirth & Kohlstedt, 1995a, b). Experiments should also be carried out either undrained (as has typically been done previously) or melt

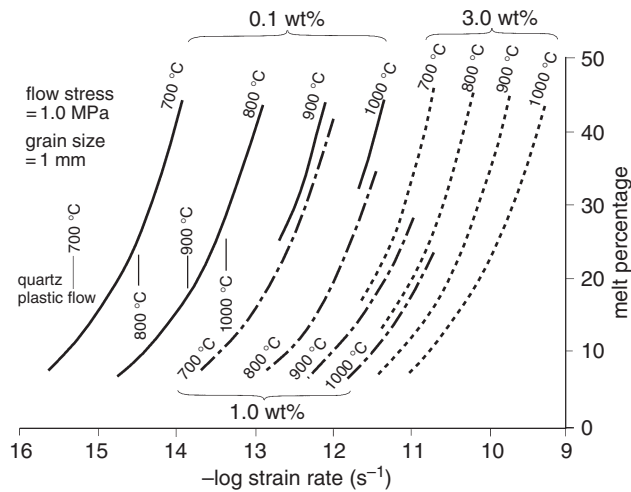


Fig. 11.6. Predictions of the model for the deformation of partially molten granite by diffusion-accommodated granular flow, showing particularly the effects of increasing temperature, water content (shown as 0.1, 1.0, and 3.0 wt.%) and melt percentage on distortional strain rate. Melt pressure assumed equal to confining pressure. All calculations made assuming a grain size of 1 mm and a constant flow stress of 1 MPa. Because the flow is linear-viscous, all curves shift one decade in strain rate to the right as stress is increased 10-fold. Assuming the rheologically critical melt percentage (RCMP) to lie at 50% melt, all curves would take a sharp deflection to the right (to much higher strain rates) above 50% melt. In all cases, over the 0–50% melt-fraction range, strength decreases by more than 100-fold. The short vertical lines at the left show strain rates expected at the same flow stress for intracrystalline plastic flow of quartz (based on the Paterson & Luan (1990) “average” flow law for quartzite). At all temperatures, the partially molten rock flows substantially faster with accommodation by diffusive mass transfer than by intracrystalline plasticity. The difference becomes more pronounced at higher temperatures and at lower stresses.

pressure should be controlled independently of confining pressure (drained). Here, we describe briefly a preliminary attempt at this approach under undrained conditions, using a peralkaline ($\text{SiO}_2\text{--Al}_2\text{O}_3\text{--Na}_2\text{O}$) melt phase (Mecklenburgh & Rutter, 2003).

Samples were fabricated with quartz as the only solid phase, mixed with the peralkaline glass formed by fusing alumina, silica, and sodium carbonate in appropriate proportions at atmospheric pressure. The eutectic temperature of the dry albite–quartz system is at 1076 °C at 300 MPa (Wen & Nekvasil, 1994), but deformation experiments must be performed at slightly higher temperatures than this (1100 and 1150 °C were used). This is to prevent albite crystallizing, but at the price of causing silica of the solid phase to dissolve in the melt,

increasing melt fraction and its viscosity. The latter effect may be offset partially with addition of a higher sodium fraction, which also helps compensate for sodium volatilization during initial fusion. Electron microprobe analysis of $[\text{SiO}_2/(\text{SiO}_2 + \text{Al}_2\text{O}_3)]$ in the melt after deformation showed an average increase from an initial 80, to 87 wt.%, and melt fractions measured after each experiment were always greater than the proportion of glass initially added. Adding water has the effect of lowering the solidus temperature and decreasing the melt viscosity.

Relatively large quartz grain sizes (around $100\ \mu\text{m}$, compared to $10\ \mu\text{m}$ in olivine + MORB experiments) must also be used with dry siliceous melts, so that viscous flow between grains was not impeded to the extent that it might become deformation-rate controlling in experiments that were aimed at studying diffusion-accommodated granular flow. Unfortunately, large grain size leads to problems of impingement grain fracture during initial pressurization and the early stages of hot pressing when the desired melt fraction is less than 45 vol.% (the porosity of a cold-pressed granular aggregate) and void spaces exist, hence confining pressure has to be incremented in a stepwise fashion during initial fusion and compaction to minimize fracturing. Large grain size unfortunately also mitigates against diffusive mass transfer-controlled flow, although for high melt-fraction samples it is the (smaller) diameter of the contact points between grains that is more important than the mean grain size.

Figures 11.7 and 11.8 show typical experimental results for dry samples. Stress–strain curves at $1100\ ^\circ\text{C}$ (Fig. 11.7) show characteristics of steady state ductile flow, and how increase in melt fraction and decrease of strain rate both reduce strength. Effects of strain rate variations are also illustrated in Fig. 11.8. The average flow stress decreases with stress in constant strain rate experiments according to a power law, with the stress exponent approximately 3.5 (c.f., the behavior of Westerly granite, Eq. (11.4)). The predicted flow behavior according to the diffusion-accommodated granular flow theory (Eq. (11.5)) for the dry system is also illustrated in Fig. 11.8. It lies outside the range of the constant strain-rate experiments performed to date, and even beyond their extension to lower strain rates using stress-relaxation testing. Addition of water also reduced strength, and stress relaxation tests showed a faster rate of decrease of strength with strain rate when wet, even though the experiments were run at a lower temperature of $980\ ^\circ\text{C}$ (to maintain a small temperature difference with respect to the reduced eutectic temperature for the wet melt). The apparent stress exponent is still about 2 rather than the predicted unity for diffusion-controlled flow, but the experimental strain rates are probably still too high to evaluate the predictions of the theory. Tests on samples with larger

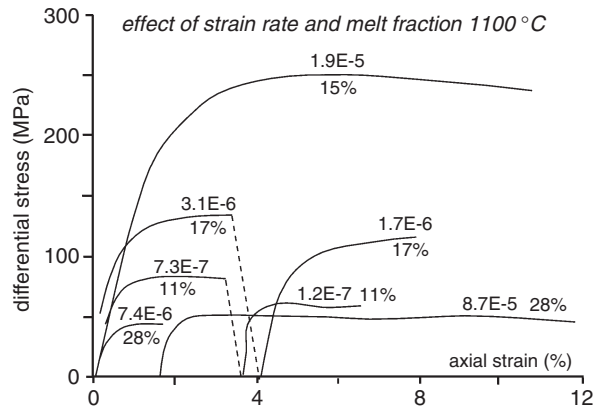


Fig. 11.7. Experimental data (undrained) at 300 MPa confining pressure and 1100 °C illustrating the effects of strain rate and melt fraction on the behavior of “synthetic” granite of 60–100 μm quartz grain size with an albite-quartz melt phase. Against each stress–strain curve is shown strain rate and melt fraction (% + 4%). The weakening effect of strain rate reduction at comparable melt fractions is apparent, and of increasing the melt fraction to 28%. Dashed lines link segments of strain rate stepping tests. (After Mecklenburgh & Rutter, 2003.)

added water fractions and smaller grain sizes will probably be required adequately to evaluate the theory.

Microstructures observed in these experimental samples are not straightforward to interpret (e.g., Fig. 11.9). There is some fracturing of grains, although it is difficult to separate fracturing during high-temperature deformation from that produced earlier, during hot pressing. Open porosity is totally absent, and only a slight preferred orientation of elongate grains was produced in samples deformed at high differential stresses (Mecklenburgh & Rutter, 2003). Grain boundaries are characterized by uneven overgrowths of new quartz and/or solution pitting, but unequivocal evidence of indentation of one grain by another is lacking. Large numbers of small, new quartz grains are produced in the melt. These are rounded or slightly faceted. Most grain interfaces appear to contain melt, although it is impossible from scanning electron microscope images to say whether the main loadbearing contacts contain melt. In these experiments, typically 10% or more strain was accumulated; hence, the microstructures appear to be consistent with most strain being accommodated by sliding of grains over one another. It is tentatively suggested that, given the non-linearity observed in the log stress versus log strain rate behavior, deformation rate in these experiments may be controlled by brittle rupture of sintered grain contacts (Mecklenburgh & Rutter, 2003).

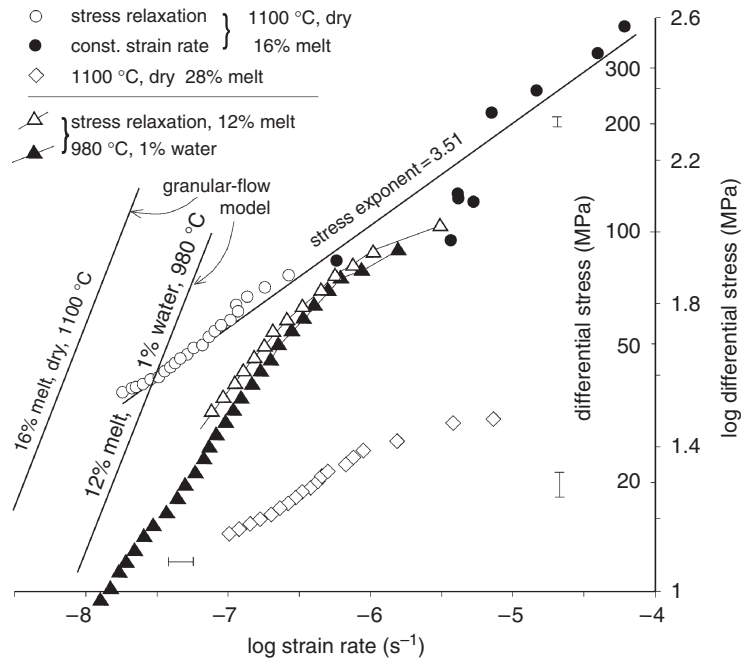


Fig. 11.8. Experimental data (undrained) at 300 MPa confining pressure illustrating the behavior of “synthetic” granite of 60–100 μm quartz grain size with an albite-quartz melt phase. “Dry” data at 1100 $^{\circ}\text{C}$ with 16 and 28% melt (constant strain rate and stress relaxation experiments) show a fairly steady rate of reduction of strength with reducing strain rate corresponding to a stress exponent of about 3.5. The strength at the higher melt fraction is much reduced. For 12% melt but with 1 wt.% water added and at a lower temperature, the more rapid rate of strength reduction corresponds to a stress exponent of about 2. These data are compared with predictions of the theoretical model for diffusion-accommodated granular flow (Rutter, 1997, stress exponent = 1) with corresponding melt fractions and water contents. (After Mecklenburgh & Rutter, 2003.)

11.4 Discussion

11.4.1 Comparability between partially molten rocks and water saturated soils

The mechanics of a water saturated granular aggregate such as a soil or a weakly cemented rock may be expected to be comparable to the mechanics of partially molten rocks. Soil deformation under undrained conditions is effectively a constant volume deformation, but under drained conditions the matrix of solid grains may compact, expelling fluid, or dilate, sucking fluid or dropping the fluid pressure. However, whereas volumetric compaction of soil takes

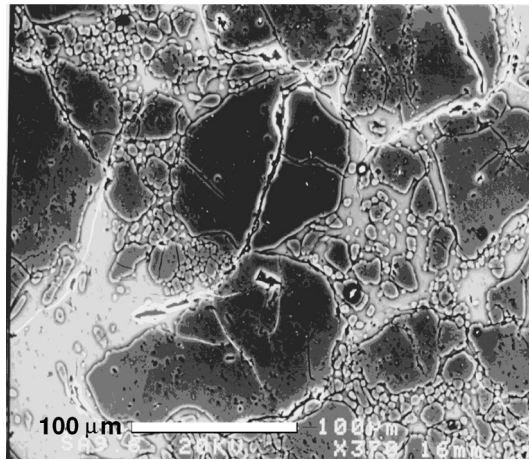


Fig. 11.9. Microstructure of an experimentally deformed synthetic quartz–quartz–albite melt aggregate (dry). The specimen was axisymmetrically shortened 12% in the vertical direction at 1100 °C at a strain rate of $8 \times 10^{-6} \text{ s}^{-1}$. There is little melt-filled fracturing of the quartz grains (dark gray), zero vapor-filled porosity, and growth of new, small quartz grains in the melt phase (light gray, 28% volume). The empty (black) cracks in the quartz are probably quench cracks. Time at temperature = 50 h.

place only by geometric rearrangement of the rigid solid particles, in a partially molten rock at high temperature the individual grains of the rock matrix may deform permanently, with the possibility of total compaction and melt elimination. Compaction may take place driven by gravity, due to the density contrast (about 400 kg m^{-3}) between melt and solids, or it may be driven by tectonic forces.

Soils behave in an elastic-plastic manner; thus, they deform only elastically and recoverably at combinations of shear and normal stress that lie below the yield surface, at which deformation occurs at whatever is the imposed rate. They also obey the law of effective stress, whereby all effective normal stress components, σ'_i (where i designates the i th component) are reduced from the applied normal stress components, σ_i , by an amount proportional to the pore pressure, p :

$$\sigma'_i = \sigma_i - \kappa p. \quad (11.11)$$

The constant of proportionality, κ , is unity when describing permanent failure, or is less than unity when describing elastic deformations. Note that shear stress components are unaffected by changes in pore fluid pressure. This law is expected to apply to partially molten rocks also, although this has not yet been demonstrated experimentally. Thus, the effective stress state may be changed

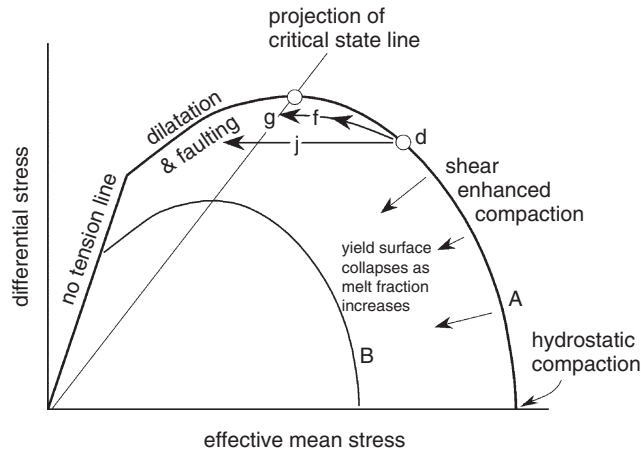


Fig. 11.10. Schematic representation of the yield surface for a porous rock. The yield surface forms a closed loop, the size of which shrinks as porosity increases (e.g., from curve A to curve B). The projection of the critical state line is the projection of the crest of successive yield loops (e.g., small circle at intersection with crest of loop A) at different porosities (Muir Wood, 1990). To the left of this line (Hvorslev region) the deformation is dilatant, and tends to result in localized faulting. To the right it is compactive (Roscoe region) and tends to result in distributed, ductile flow. Yield is possible even on the abscissa if the effective hydrostatic pressure is sufficient to initiate pore collapse and any pore fluid may be expelled. Variations in pore fluid (melt) pressure cause effective pressure changes and, hence, behavioral changes. For example, from the small circle labeled d on curve A, progressive compaction during failure may lead to a displacement of effective stress to the left (path f) until isovolumetric failure is achieved at g, or pore pressure rise (path j) at constant differential stress, perhaps from melt influx from beneath, may displace the stress state to the left until dilatant yield (faulting) is produced.

as a result of changes in pore pressure (that may be related to drainage, for example), with consequent effects on the mechanical behavior.

The yield surface for a soil or porous rock is usually represented on a diagram that plots differential stress ($\sigma_1 - \sigma_3$) against effective mean stress ($\sigma - p$), where $\sigma = (\sigma_1 + \sigma_2 + \sigma_3)/3$ (Fig. 11.10). These are the components of a *stress vector*, and for vectors below the yield surface, no permanent deformation occurs at all. At low effective mean stress, strength increases with effective mean stress (the Hvorslev region), and this region corresponds to Mohr–Coulomb failure behavior, which is accompanied by dilatancy and a tendency for deformation to occur by localized brittle shear failure. This causes fluid pressure to fall, thereby tending to increase effective stress. The stress vector moves to the right, below the yield surface, inhibiting further deformation unless more differential stress is applied or until fluid pressure is

restored by drainage into the dilatant region (dilatancy hardening). The Hvorslev region is bounded to the left by a line with slope = 3, which corresponds to the presumed inability of the material to sustain effective tensile stresses. In this region of high fluid pressure, extensional, fluid-filled fractures are likely to form.

It is reasonable to suppose that even under hydrostatic conditions (points along the abscissa), there will be an effective pressure at which failure by isotropic pore collapse occurs. Thus, the yield surface must loop around from the Hvorslev region, through a region of negative slope (the Roscoe region), to the point representing hydrostatic compaction. The Roscoe region corresponds to shear failure but involving compaction, under combined hydrostatic and shear stress, and is sometimes called the region of shear-enhanced compaction (Curran & Carroll, 1979). At the point at the crest of the yield surface, where the slope is zero, dilatancy and compaction are balanced, and distortional flow occurs at constant volume (critical state). Granular materials require higher effective stresses to induce hydrostatic compaction if porosity is low; hence, the size of the yield surface increases as porosity decreases (Fig. 11.10). Therefore, as yield occurs in the compactive region, the porosity decreases, causing the yield surface to expand (strain hardening). Thus, a higher combination of stresses (a longer stress vector) must be applied to keep the deformation going. Such local hardening should tend to spread the failure uniformly throughout the material and, hence, to promote macroscopic ductility. Conversely, dilatant deformation (in the Hvorslev region) should tend to result in localization of the flow into a shear band.

Failure changes the properties of the deforming material by changing the porosity. Changes in pore pressure, according to whether the solid framework dilates or compacts, consequently change the effective stress state. Hence, during deformation, the tip of the stress vector is forced to migrate over the evolving yield surface. In the context of the axisymmetric loading configuration under confining pressure σ_3 , as is used in experimental studies, the change in pore fluid pressure, δp , in response to a change in confining pressure or differential stress is given by Skempton's (1954) equation

$$\delta p = B\delta\sigma_3 + A\delta(\sigma_1 - \sigma_3). \quad (11.12)$$

For a fully saturated aggregate, $B = 1$, but A may be either positive or negative, according to whether loading by differential stress induces dilatation or compaction, which is, in turn, largely determined by the magnitude of the effective mean pressure (e.g., Smith, 1990). The magnitude and sign of A may evolve during a single deformation episode. Thus, the magnitude of A describes the capacity for local gradients in shear stress to induce corresponding variations

in pore pressure, and for tectonic stress gradients to provide a driving force for melt migration.

For rocks and soils at low temperature, the size of the yield surface does not change with time or strain rate, but with strain as porosity evolves. However, at high temperatures, thermally activated creep will cause the effective size of the yield surface to vary with strain rate, becoming very small for slow deformations (i.e., time-dependent isotropic compaction may occur under very small effective pressures, such as <1 MPa). This implies that local variations of shear stress may be only of the same order, or less, and this is a measure of the contribution that tectonic stresses may make to the driving force for melt migration. It is interesting to compare this with the magnitude of gravity induced pressure gradients that drive melt migration. Local melt pressure differences driving flow are likely to be on the order of

$$\delta p = (\rho_s - \rho_f)gz, \quad (11.13)$$

where ρ_s is the density of the melt free solid, and ρ_f is the density of the crystallite-free melt, g is the gravitational acceleration, and z is the height of the melt-containing column of crust, such as the length of a dike. Thus, for typical crustal rock density contrasts, $dp/dz \sim 0.003 \text{ MPa m}^{-1}$. The longer a vertical dike becomes, the greater will be the driving force that pushes melt into the dike base. If the flow strength of a partially molten rock is around 1 MPa, it is likely that tectonic stress differences driving melt migration will be of the same order. If a gradient of 1 MPa is developed over a distance of the order of from 1 to 10 m, this would represent a substantial (from 100 to 1000 times) enhancement relative to the gravity induced pressure gradient. But if that variation is spread over 1 km or more, then the influence of tectonic stress as a driving force for melt migration may be no more, and probably much less, than the gravity induced gradient.

11.4.2 Viscosity of the melt phase and rheologically critical melt percentage

If, in an experiment, a partially molten rock like Westerly granite could support 1 MPa differential stress at a laboratory strain rate of 10^{-5} s^{-1} , with 48 vol.% of the rock mass molten, this would correspond to a bulk viscosity on the order of 10^{11} Pa s . Thus, although such a rock would be weak by solid-state flow standards, it would remain a strong rock compared to the viscosity of the permeating liquid (at most 10^8 Pa s). Lejeune and Richet (1995) showed how, at low crystallite fractions, effective viscosity of a melt–crystal suspension increased by approximately $\times 10$ in association with an increase in crystallite fraction to 42 vol.% (for an aluminous enstatite melt with a crystallite-free

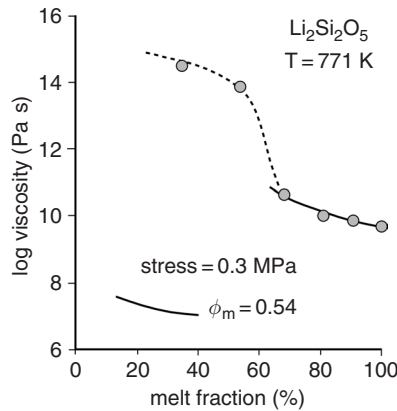


Fig. 11.11. Experimental data of Lejeune and Richet (1995) that illustrate particularly effectively the concept of RCMP, at about 55% melt, for lithium silicate. At high melt fractions, the stiffening effect of increasing crystallite fraction may be described well by the Einstein–Roscoe equation with a critical melt fraction of 54% and an exponent of 2.5. At lower melt fractions (below 54%) there is a dramatic strengthening (RCMP) corresponding to impingement of crystallites and transition to a more nonlinear bulk rheology. At even lower melt fractions, there is still an implied strong sensitivity of viscosity to melt fraction, in the same way as observed for partially molten granitic rocks.

viscosity of 4×10^9 Pa s). In this regime (Fig. 11.11), the behavior is described fairly well by the Einstein–Roscoe equation (Roscoe, 1952):

$$\eta = \eta_0 \left[1 - \frac{1 - \phi}{1 - \phi_m} \right]^{-q}, \tag{11.14}$$

in which η is viscosity, η_0 is viscosity without suspended particles, ϕ the volume fraction of melt, q is an exponent of order 2.5 and ϕ_m is the melt volume fraction for a packed aggregate of grains that may support load, for which the porosity depends on crystallite size and shape distribution. In this range, the viscosity of the suspension also remains linearly viscous (i.e., the strain rate increases linearly with applied shear stress. However, between a crystallite volume fraction $[(1 - \phi) \times 100]$ of 40–60 vol.%, the viscosity was observed to increase by 3 orders of magnitude (Fig. 11.11), deviating sharply from the predictions of the Einstein–Roscoe equation. This jump corresponds to what has been termed the rheologically critical melt percentage (RCMP), the melt fraction beyond which the contiguity of the solid framework of grains breaks down, and grains begin to be carried in the viscous melt. The linearity of stress versus strain rate also breaks down, with strain rate becoming more sensitive to small changes in stress.

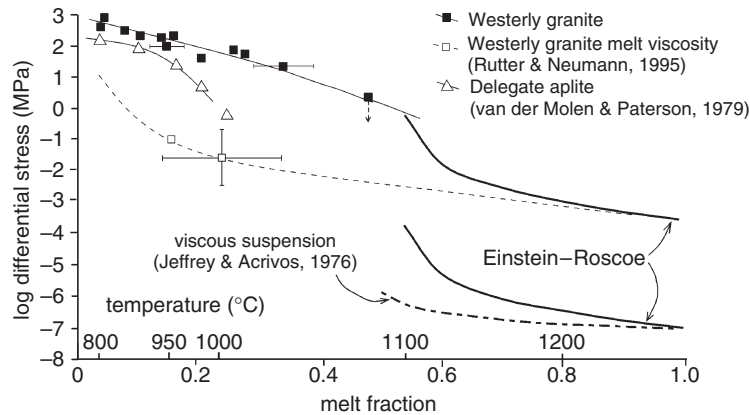


Fig. 11.12. Experimental data of Rutter and Neumann (1995) for partially molten Westerly granite and of van der Molen and Paterson (1979) for Delegate aplite showing the large decrease in strength observed with increasing melt-fraction in both cases. For Westerly granite, melt fraction was increased by increasing the temperature. In the case of Delegate aplite, it was increased by increasing water content at a constant temperature of 800 °C. Although the strength of the aplite decreases more rapidly with melt fraction, note the logarithmic strength scale, and the fact that both rocks weaken by about 500-fold over the observed melt-fraction range. Note that the lowest strength data point for the aplite was determined from reconstituted crushed rock, and that the melt viscosity varies much more over the observed melt fraction range in the case of the aplite than for the granite. Open squares show upper bounds on the viscosity of the Westerly granite melt, extrapolated to its high temperature value, when the rock would be expected to be fully molten. Bold, continuous curves show bulk viscosity calculated for melt-crystal suspensions using the Einstein-Roscoe equation, assuming in each case a critical melt fraction of 50 and 100% melt viscosities of 10^4 and 3×10^7 Pa s for Delegate aplite and Westerly granite melts, respectively. Bulk viscosity variation experimentally determined (Jeffrey & Acrivos, 1976) for a suspension with liquid viscosity of 10^4 Pa s is also shown for comparison. The Westerly granite data therefore are compatible with an RCMP of about 50% melt, or perhaps at a slightly lower melt fraction in the case of Delegate aplite.

The relation between the flow stress and melt fraction for partially molten grantoids at low melt fractions as observed by Rutter and Neumann (1995) and van der Molen and Paterson (1979), compared to the viscosity of the pure melt, is shown in Fig. 11.12. The results of van der Molen and Paterson (1979) for Delegate aplite, involving an acceleration of rate of fall in flow strength with melt fraction, even when plotted on a logarithmic strength scale, were interpreted by them in terms of the existence of an RCMP, at a melt fraction of only 25–35 vol.%. Note that the substantial strength drop (approximately $\times 500$) with increasing melt fraction that is observed in both the above

sets of experiments, is smaller than the further implied strength drop (from $\times 10^3$ to 10^4) as solid grain contiguity is lost at a melt fraction of about 45–50 vol.%. The trend at low melt fractions for Westerly granite suggests an RCMP may lie at a melt fraction not less than 48 vol.%, which would be consistent with the results of Lejeune and Richet (1995). In their experiments, van der Molen and Paterson (1979) increased water content in order to increase melt fraction at constant temperature (800 °C), whereas in the Rutter and Neumann (1995) experiments, water content remained constant and melt fraction was increased by increasing temperature. In the former case, melt viscosity was much lower than in the latter, and decreased much more strongly with increasing water content than it would with increasing temperature.

Renner *et al.* (2000) suggest that the difference between these two sets of results may be attributable to the effects of dilatancy hardening (Brace & Martin, 1968; Rutter, 1972). A combination of low permeability, high pore fluid viscosity and high strain rate during rock deformation by a mechanism that may involve dilatancy (such as cataclasis and granular flow), may lead to the pore pressure falling transiently, with concomitant strengthening of the rock (dilatancy-hardening). A lower strain rate, favoring less dilatancy, and allowing more time for the viscous pore fluid to flow in response to local pore volume fluctuation, may allow the pore pressure to remain fully effective everywhere at all times. Thus, the high strength of partially molten granite at low melt fractions (when permeability is low) may be due to a high effective confining pressure, and the rapid decrease in strength with increasing melt fraction may be due to progressively decreasing effective confining pressure, until it becomes zero when melt may flow freely around grains. Delegate aplite, with its lower melt viscosity, would be more likely to display a wide variation in strength at laboratory strain rates and moderate melt fractions than Westerly granite and, hence, to give the appearance of an RCMP at lower melt fractions than the expected values of 45–50%. Dilatancy-hardening might also be partially responsible for the commonly observed phenomenon of an initial high yield strength followed by strain weakening that is commonly observed for partially molten granitic rocks.

Renner *et al.* (2000) also suggested that the persistence of relatively high strength of Westerly granite to higher melt fractions than for Delegate aplite might be due to dilatancy-hardening in a material with a higher melt viscosity. However, the different behavior of these two granites cannot be explained in this way because, in virtually all experiments on natural granites, solid–melt equilibrium was not attained, and during the course of each test the melt fraction increased by as much as several percent, thereby counteracting the effect of dilatancy on the melt pressure. By measuring melt fraction as a

function of time, Rutter and Neumann (1995) estimated that at least a year would be required to attain an equilibrium melt fraction.

The “true” RCMP (due to the physical unlocking of the matrix of solid grains) is held widely to be of great importance for the behavior of partially molten rocks. The strength of migmatitic rocks in a tectonically active regime, even at melt fractions less than the RCMP, is expected to be very low compared to the intracrystalline-plastic flow strength of solid rocks. Thus, a migmatite that is trapped between impermeable solid crustal rock units above and below has effectively zero strength, and will be extremely effective as a zone of detachment, separating tectonic processes above from those below. Snoke *et al.* (1999) describe such a large-scale, melt-lubricated shear zone (1 km thick and extending 30 km along strike) in migmatitic rocks overlying a 10-km thick mafic sill of Permian age emplaced into lower crustal rocks in the Ivrea–Verbano zone in the Alps of northern Italy.

11.4.3 Microstructural considerations

What do the structure and microstructure of naturally deformed, partially molten rocks tell us about deformation mechanisms and the permeability of those rocks? Grain-shape preferred orientations are commonly seen in granitic rocks, such as the orientation of plates of idiomorphic feldspar crystals. The *shape* of idiomorphic crystals probably implies surface energy equilibration with respect to a melt phase, and the *preferred orientation* (of platy or prismatic crystals) suggests that some degree of granular flow had occurred. Such crystals also may demonstrate that diffusion-creep has occurred when they are seen to be interpenetrated or eroded in contact with neighboring crystals (Park & Means, 1996; Nicolas & Ildefonse, 1996; Rosenberg, 2001).

Granular flow is also implied in localized, melt-pervaded, shear zones in which there is evidence of dilatation in the form of a greater melt fraction than in the host rock. Granular flow is expected to be dilatant if diffusive mass transfer does not keep pace with the imposed rate of shear, or if deformation is accommodated by friction and fracturing of grains. The driving force for such dilatation is the shear stress on the aggregate, and because this is expected to be small (at low strain rates) compared to the total mean stress on the aggregate, the dilatation may occur only if the system is very nearly undrained. That is, the melt pressure is very nearly equal to the total mean stress; hence, the effective stresses are very small.

Recent detailed studies of melt distributions and interconnectivity on the grain scale and above have begun to demonstrate the ways that the formation and drainage of melt in natural anatectites at these scales is controlled by

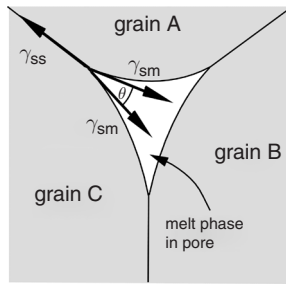


Fig. 11.13. Illustration of the control exerted by interfacial energy (γ_{sm} (solid–melt) or γ_{ss} (solid–solid)) on the shape of melt volumes (white) when at hydrostatic equilibrium. If $\theta > 60^\circ$ is forced to reside at four-grain junctions or as isolated blebs along three-grain junctions. If $\theta < 60^\circ$, continuous melt channels may exist along all three-grain edges, leading to permeability. If $\theta = 0^\circ$, melt wets all grain interfaces. Note that for anisotropic materials, θ may vary with crystallite orientation.

lithological factors, local finite strain, or differential stress states (Brown *et al.*, 1999; Sawyer, 2001; Marchildon & Brown, 2002; Rosenberg & Handy, 2002; Holtzman *et al.*, 2003a, b). It may be unusual for such textures and microstructures to be preserved at the grain scale in naturally partially melted rocks, which may be subject to later or penecontemporaneous microstructural readjustments.

Interconnectivity of liquid filled volume may be substantially enhanced in a localized shear zone, thereby providing an enhanced permeability pathway for melt through the granular matrix (Zimmerman *et al.*, 1999; Bruhn *et al.*, 2000; Rosenberg & Handy, 2000; Rosenberg, 2001). This may be particularly important at low (<10 vol.%) melt fractions if: (1) equilibrium surface energy relations tend to develop between crystals and matrix, and (2) the equilibrium dihedral angle between melt and solids is relatively large, which tends to result in low permeability. Under hydrostatic (isotropic) stress, the microstructure of the partially molten aggregate is expected to tend towards an equilibrium in which the dihedral angle, θ , between two adjacent grains (Fig. 11.13) is determined by the relative interfacial energies between melt and solid (γ_{sm}) and between solid and solid (γ_{ss}):

$$\gamma_{sm}/\gamma_{ss} = 2 \cos(\theta/2). \quad (11.15)$$

Note that an apparent equilibrium dihedral angle of several tens of degrees does not necessarily preclude the stable existence of nanoscale melt films in a stressed interface (Clarke, 1987; Drury & Fitzgerald, 1996; Hess, 1994). For $\theta > 60$, the melt is expected to be confined to four-grain corners, and three-grain

edges will not be continuously wetted; hence, the melt phase will not be interconnected, and permeability will be zero. For smaller θ values, the melt phase will interconnect along the three-grain edges and permeability will be finite, increasing as the total melt fraction increases. This tends to be true for partially molten granitic rocks (e.g., Laporte, 1994). This rule may be relaxed somewhat by taking into account the anisotropy of surface energy that tends to characterize low-symmetry silicate structures. Waff and Faul (1992) point out that (010) faces in olivine are preferentially wetted by melt; hence, the permeability may be enhanced if intracrystalline plastic flow results in a crystallographic preferred orientation of the solid framework, or if crystals of platy habit become oriented during granular flow.

It should be noted that a crystallographic fabric may be produced by solid-state flow prior to melting, and there may not necessarily be an implication that deformation of the partially molten rock involved intracrystalline plastic flow of the solid framework. Although it is difficult to find unequivocal evidence that solid phases in a granitic rock underwent intracrystalline deformation in the presence of melt, Gapais and Barbarin (1986) and Rosenberg and Riller (2000) report careful microstructural studies that support such an inference.

Apart from studies on analog materials (Rosenberg & Handy, 2000; Rosenberg, 2001), experimental evidence from high-temperature–high-pressure studies for the focusing of melt into dilatant shear zones is presently only available for olivine aggregates pervaded with basaltic melt (Zimmerman *et al.*, 1999; Holtzman *et al.*, 2003a, b), olivine with albite melt and anorthite with basaltic melt (Holtzman *et al.*, 2003a), or olivine with molten metals or metal sulphides (Bruhn *et al.*, 2000) deformed in forced shear zones. In all cases, interconnected sub-planar melt arrays formed in the sheared volume at about 10–30° to the shear direction (Fig. 11.14a, b), whereas isolated melt pockets tended to form in hydrostatically stressed samples. Holtzman *et al.* (2003b) found that the strain partitioning that accompanies melt segregation into shear bands influences the pattern of crystallographic-preferred orientation that developed as a result of the intracrystalline plastic flow of the olivine matrix. This has implications for the seismic anisotropy that might develop during flow of partially molten mantle rocks.

In axially symmetric compression experiments, Bussod and Christie (1991) and Daines and Kohlstedt (1997) noted a tendency for melt to become preferentially concentrated into grain boundaries oriented at 20–30° to the compression direction, and Jin *et al.* (1994) have observed that deformation of partially molten ultramafic rocks results in the break-up of isolated melt pockets, enhanced redistribution of melt, and spreading around grain

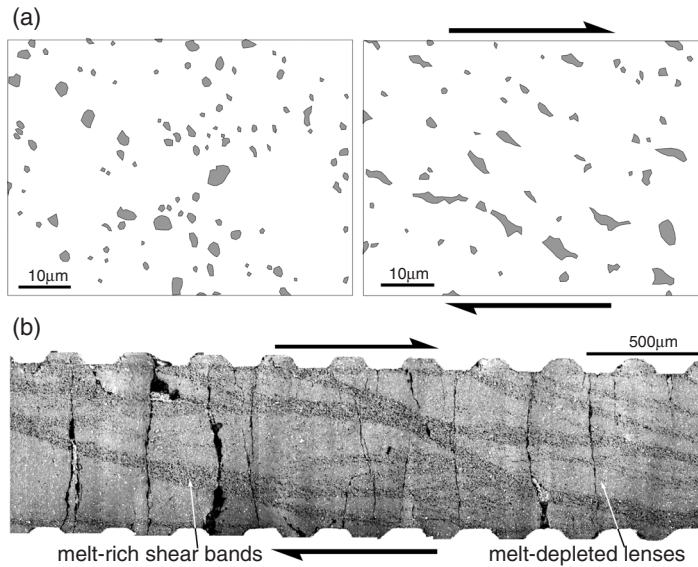


Fig. 11.14. (a) Tracings of optical micrographs comparing undeformed (left) and sheared (right) samples of hot-pressed olivine with a metal sulfide melt phase (7 vol.%, gray shaded) from experiments at 1250 °C under undrained conditions reported by Bruhn *et al.* (2000). The undeformed sample shows isolated melt pockets with large dihedral angles; hence, zero permeability. Deformation causes segregation of melt into fewer, larger, melt pockets, preferentially oriented about 20° to the shear direction, the existence of which implies deformation-enhanced connectivity. Reconstruction of the 3-D structure by serial sectioning showed these to be well-connected sheets of molten material extending into the third dimension. (b) SEM image of sheared fine-grained (3 μm) olivine + chromite matrix with 4% basaltic melt, showing segregation of melt (black) into dilatant shear bands oriented about 20° to the bulk shear direction, leaving lenses of melt-depleted matrix (shear strain = 3.5, flow stress 30–60 MPa). The vertical black cracks were induced during specimen recovery, and the stepping of the top and bottom of the sheared sample corresponds to steps in the forcing pistons made to minimize slip at the edges of the sample. (Photo courtesy of B. Holtzman.)

boundaries. These examples all involve dilatation of grain boundaries. Most experimental studies on the axisymmetric deformation of partially molten granitic rocks (e.g., Rutter & Neumann, 1995) at differential stresses sufficiently large to produce fracturing of grains, have noted the drainage of melt into such fractures or into similarly oriented dilated grain boundaries (Gleason *et al.*, 1999).

Both experimental studies and observations of dilatation and focusing of melt into localized shear zones (e.g., D’Lemos *et al.*, 1992; Vigneresse, 1995; Fig.11.15) demonstrate that granular flow under non-hydrostatic stress is

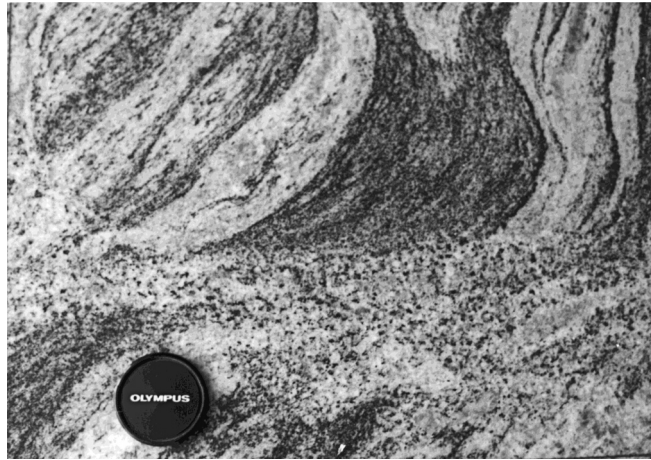


Fig. 11.15. Photograph of a natural migmatite showing preferential concentration of melt phase (now crystallized as fine-grained granite) into a ductile shear zone (origin of sample unknown). Diameter of lens cap is 5 cm.

important in nature, and that such localized deformation may be important in the drainage of melt and its accumulation as the first step in the formation of plutons. It is also clear that fracturing may be an important process for tapping melts. A three-dimensional network of fractures or of localized dilatant shear zones may enhance the effective permeability of a partially molten rock mass by several orders of magnitude (cf., Chapter 10).

11.4.4 Permeability of partially molten rocks

It is usual to assume that the factors governing the permeability of partially molten rocks are the same as those governing the permeability of solid rocks to water at low temperatures. In texturally equilibrated rock, flow may occur pervasively at the grain scale, along three-grain edges with the geometry of the conductive channels controlled by the wetting relations between solid and liquid phases, or individual grain boundaries may dilate under tectonic stresses. Partially molten rocks may also develop mesoscale fracture networks or other extensional failure features such as interboudin partitions that may become filled with melt. If they are interconnected, they may become very effective drainage pathways. For either case, simple permeability models may be erected, linking, on the one hand, intergranular porosity and grain size to permeability, or, on the other, crack porosity and average crack spacing and opening aperture (or other more sophisticated statistical descriptions of crack array geometry) to permeability.

A simple but widely used expression for grain scale permeability, k , is

$$k = d^2 \phi^r / C, \quad (11.16)$$

in which d is mean grain diameter, and C is a dimensionless number, the value of which depends on pore geometry, which may be derived theoretically or empirically. For the case of Fontainebleau sandstone, the data of Bourbie and Zinzner (1985) give $C \sim 400$ and $r = 3$. For flow through a network of planar veins, one may take as a starting-point the result for the mean flow velocity U for flow in a parallel-sided channel of width s under a pressure gradient dp/dx

$$U = \frac{-s^2 dp}{12\eta dx}. \quad (11.17)$$

For a parallel array of N channels per meter, this is analogous to Darcy's law with permeability given by

$$k = Ns^3/12. \quad (11.18)$$

The crack porosity of the network is Ns . A more complex arrangement of channels will affect the permeability by a numerical factor. For the same crack porosity, one wide crack is more effective than many narrow cracks.

It is instructive to compare grain scale permeability with that due to a crack network, for the same porosity. Assuming a grain size of 5 mm and a melt fraction, ϕ , of 10 vol.%, grain scale permeability is $6 \times 10^{-11} \text{ m}^{-2}$, whereas for a crack spacing of 500 mm, the crack permeability is $2 \times 10^{-5} \text{ m}^{-2}$. Even a low-density crack array forms a much more effective drainage network than flow through pore spaces. Once melt has been gathered into cracks and veins, the enhanced permeability of crack arrays allows even high viscosity melts to flow at significant rates.

11.4.5 Extraction of granitic melts from their protoliths

Brown *et al.* (1995) identify three principal contributions to the driving forces for melt extraction: (1) gravity driven compaction of the solid matrix, causing upward drainage of melt; (2) forces arising from volume changes associated with melting (expansion–contraction convection), and (3) melt segregation assisted by differential stress. Brown *et al.* (1995) are particularly concerned with the processes involved in local segregation of melt to form stromatic migmatites, in which melt lenses (represented by leucosomes) form parallel arrays within source material (mesosome), sometimes with mafic-rich selvages (melanosome) flanking the leucosome (see Chapter 10). The latter probably

represent solid residue from partial melting reactions. In such rocks, the mesosome is often schistose; thus, the processes leading to the segregation of leucosomes and the interconnection of channels probably are influenced strongly by the mechanical anisotropy of the starting material, rather than dominantly by the applied stress (including melt pressure) state. At the other extreme, migmatites may be nearly isotropically textured, but transected by arrays of veinlets, shear zones, and other more or less irregular bodies in which melt has accumulated, which may represent fast drainage routes, ultimately feeding dikes that transport the magma to higher crustal levels. It will be argued that the development of closely spaced (of the order of 1 m) veinlets are an essential part of the ability of a partially molten granite protolith to drain its melt in a geologically reasonable time frame.

We will consider below the contributions of (1) and (3) above, but it should be noted that, in general terms, melting without added fluid phase causes a net volumetric expansion of the system, so that the excess melt volume must dilate the rock mass, creating spaces between grains, or forming mesoscopic crack arrays, including opening of pre-existing schistosity planes if present. Melting involving addition of fluid from outside, or from what is trapped in pre-existing pore spaces, results in net volume decrease, requiring some degree of compaction by permanent deformation of the framework of solid grains. Petrographically distinct layers or volumes will respond differently to these forces, leading to the potential for local segregations (process (2) above).

Brown *et al.* (1999) point out that compositions of granitic plutons suggests that the melting of 10–25 vol.% of the source region was required, implying that a pluton requires 4–10 times its own volume of protolith to have been tapped in the source region. By the time a source region has become exposed to inspection by geologists, it may have suffered any degree of drainage. Veinlets may be full, frozen in the act of supplying melt to a sink that has adventitiously been cut off, or most of the melt may have drained away, with concomitant collapse under gravity of most of the remaining melt-filled porosity and vein networks.

Production and accumulation of granitic melt are sequential processes. The slowest step will control the overall rate and affect the ultimate frozen appearance of the system. The rate of supply of heat to drive the endothermic melting reactions limits the maximum rate of production of the system. There is no requirement for a steady state to become established; thus, if the roof of the suprasolidus rock mass does not fail by fracture, and if lateral drainage pathways are also impermeable, melt fraction in intergranular spaces and in veinlets or other accumulations will increase until limited by available heat supply. In this totally undrained state, the rock will be so weak that tectonic stress

gradients will be insignificant, but the rock mass will be able to respond in a very ductile fashion to small regional stresses, and may be a very effective detachment horizon in the lower crust. If the roof or sides of such a region should become breached, this region of protolith may then be able to supply large amounts of magma to higher levels very rapidly.

If drainage is permitted concurrently with melt production (at a rate determined by the heat flux) – and assuming: (1) porous flow from intergranular regions to collecting veinlets, followed by (2) channel flow along veinlets – the melt volume (and, hence, veinlet aperture dimensions) and pressure drops in each part of the system, will adjust spontaneously by inflation with melt or compaction of the solid framework until the volume averaged melt flux everywhere in the system is the same.

It is instructive to estimate the relative ease of gravity driven porous flow between grains compared to gravity driven flow within veinlets. Widespread use has been made of results derived theoretically by McKenzie (1984, 1985), which allow an estimate to be made of the time t_h required to reduce the melt filled porosity of a layer of thickness, h , by a factor e , and the amount of melt (equivalent to a layer of thickness h_m) extracted in time t_h . These are given by

$$t_h = \tau_0 h / \delta_c \quad \text{and} \quad h_m = h \phi (e - 1) / e, \quad (11.19)$$

where δ_c is the compaction length, the height over which compaction of the solid matrix is occurring against an impermeable lower boundary (Fig. 11.16). δ_c is given by

$$\delta_c = (\mu k / \eta)^{1/2}, \quad (11.20)$$

in which μ is the effective viscosity of the solid matrix. At higher levels, the upward flux of expelled melt prevents compaction. The characteristic compaction time τ_0 , is the time required to reduce the melt fraction by a factor e at the base of the compacting layer

$$\tau_0 = \delta_c / [w_o (1 - \phi)], \quad (11.21)$$

in which w_o is the relative velocity between melt and matrix, given by

$$w_o = k(1 - \phi)(p_s - p_f)g / \eta \phi. \quad (11.22)$$

These expressions allow us to compute, for example, the time required to extract, as granite melt by porous flow, 10 vol.% melt from a protolith under the influence of gravity. Figure 11.17 compares these times as a function of temperature and water content for: (1) porous flow with a grain size of 5 mm and a permeability calculated from Eq. (11.16), and (2) drainage of a network

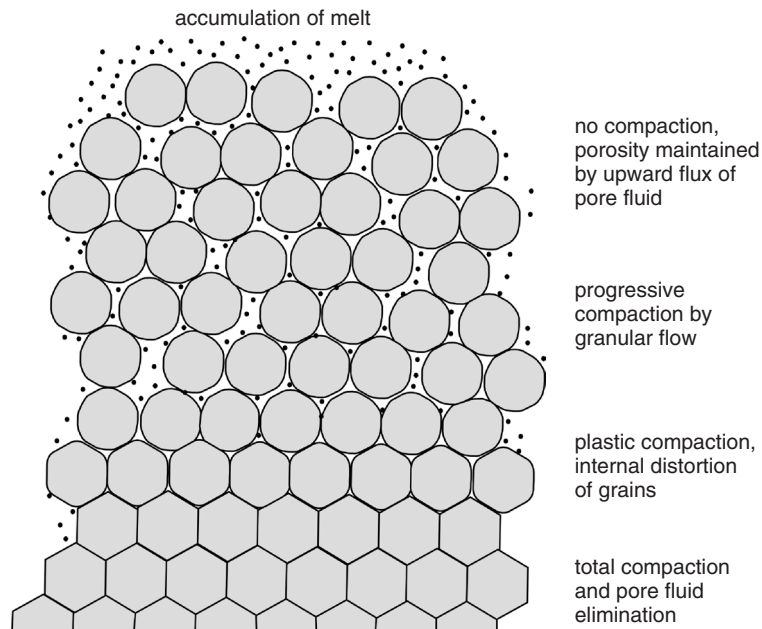


Fig. 11.16. Illustration of gravity driven extraction of melt and resultant compaction of the matrix of grains. Compaction is assumed to take place against an undeformable substrate, but everywhere the bulk stresses are hydrostatic (the lateral constraint locally equals the vertical pressure). The lowermost grains are permanently deformed either by intracrystalline plasticity or by diffusive mass transfer, to eliminate pore space. Above, there is a transition to pore space reduction by intergranular sliding. Above the compacted zone, the upward flux of melt prevents compaction, and melt eventually accumulates at the top of the section.

of veinlets that are 5 cm wide (on average) and 1 m apart. The heat source is assumed to be a mafic sill at 1200 °C lying about 500 m beneath. Melt fractions were calculated following Clemens and Vielzeuf (1987), but the water contents shown have only been assumed to affect melt viscosity, and their effect on equilibrium melt fraction beyond the point of initial melting has been neglected. It is also assumed, for simplicity, that the water content of the melt remains constant with progressive melting, whereas in reality the melt water content will decrease with progressive melting.

The effective permeability of the rock mass in case (2) is $\sim 10^6$ greater than in (1), and this accounts for the much faster rate of drainage. Except for very wet melts (>3 wt.% water), porous flow cannot lead to granitic melt extraction in geologically reasonable periods of time ($< 10^7$ years, Wickham, 1987), whereas once the melt is collected into a network of channelways such as veins,

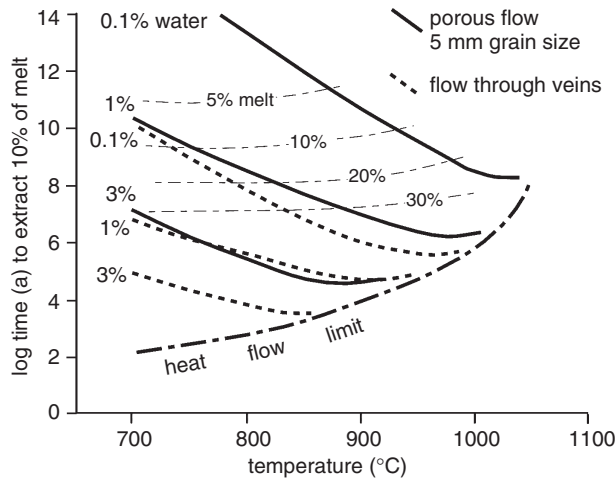


Fig. 11.17. Comparison of the time (in years) required to extract 10% of the volume of a granitic rock as melt (under gravity alone) according to: (1) the porous flow model for intergranular flow with a grain size of 5 mm (upper solid curves, labeled with melt water contents of 0.1, 1.0, and 3.0 wt.%, respectively), and (2) the porous flow model applied to a network of veinlets of volume fraction 5% (lower dashed curves for same range of melt water contents) (based on Rutter & Neumann, 1995). An upper limit to extraction rate is set by the rate that the latent heat of fusion may be supplied to the material (heat flow limit curve). Contours of melt volume fraction are also shown applying to the porous flow curves. Melt viscosities are based on the Hess and Dingwell (1996) description and melt fractions are calculated following Clemens and Vielzeuf (1987). Porous flow alone is too slow to extract melt in geologically realistic times, except for very wet melts.

interboudin partitions, or dilatant shear zones, this problem disappears. But the melt is generated at interfaces between grains on the grain scale, so porous flow is required at least initially to extract the melts into high conductivity channelways. Gravity induced vertical melt pressure gradients are too small ($\sim 0.003 \text{ MPa m}^{-1}$) to drive this intergranular flow of viscous melts.

It is in this initial process that tectonic deformation may play a part, provided differential stress gradients on the order of 1 MPa m^{-1} may arise. The melt in a veinlet cannot sustain differential stress (its viscosity is orders of magnitude less than that of the partially molten protolith for melt fractions less than 45 vol.%). We may imagine that the migmatitic rock mass is like a pile of grapes surrounded by interconnected “veinlets” of juice. Differential load may be transmitted to the grapes via their contiguous network of stationary and sliding contact surfaces, yet the entire mass is drained by the juice channels. Thus, the deviatoric stress gradient forcing juice from the grapes into the channels is of the

order of the far-field applied stress divided by the grape diameter. In migmatite terms, this is the far-field differential stress (of the order of 1 MPa or less) divided by the channel separation (of the order of 1 m). Hence, the stronger the rock mass (i.e., at smaller melt fractions), the greater is the momentum that the tectonic stress may impart to the melt. The enhancing effect of a higher strength at lower melt fractions is partially offset by the lower permeability at lower melt fractions. Lower melt fraction also may imply lower temperature and, hence, higher melt viscosity that also helps offset the effect of the higher strength. For realistic variations of melt fraction and viscosity with temperature, increasing temperature always increases the rate of deformation-enhanced melt extraction.

Rutter and Neumann (1995) described a model for the expulsion of melt into veins in a simplified way. Melt-producing rock volumes of permeability k and mean diameter $2a$ (the separation between veinlets) are subject to a far-field differential stress σ_a . Assuming a steady state, so that the geometry remains constant over a period of time, the rate of production of melt ϕ is the same everywhere and equals the rate of melt loss to the veins. Poisson's equation must then be satisfied for the pore pressure p :

$$\nabla^2 p = \phi \eta / k. \tag{11.23}$$

The solution to this equation (Rutter & Neumann, 1995) gives the radial distribution of melt pressure in the fluid filled pore spaces between the veinlets. By incorporating into the solution the requirements of mechanical equilibrium, and making the arbitrary simplifying assumption that local pore pressure is raised above the pressure in the veins by one-third the local differential stress (i.e., $A = 1/3$ in Eq. (11.12)), the rate of stress-assisted supply of melt to the veins is given by

$$\dot{\phi} = 8k\sigma_a / 3a^2\eta. \tag{11.24}$$

In this expression, ϕ includes any time-dependent generation of melt according to the heat flux and the stress-induced compaction of pore spaces. The rate of loss of the melt is then limited by viscosity and permeability and driven by the stress-induced elevation of melt pressure. Thus, the flux is determined by the requirement to maintain a steady state to match the permeability and viscosity terms. In practice, the rheology of the solid matrix limits the rate at which it may collapse and expel melt. Modifying Eq. (11.24) to include, for example, a rheology determined by diffusion-accommodated grain boundary sliding, reduces somewhat the predicted melt expulsion rate, effectively by reducing the value of the empirical parameter A and making it temperature-dependent.

The two processes: (1) supply of melt to veins or other drainage channels, and (2) gravity driven drainage of those channels, are sequential processes, so

the slower one controls the overall rate. In practice, the amount of inflation of the channel network and, hence, its permeability, is expected to adjust until the two rates become equal. Substituting $Ns^3/12$ (Eq. (11.18), for a simple representation of permeability due to flow through veinlets) into Eq. (11.22), the rate of melt separation under the influence of gravity may be written as

$$\phi \approx Ns^3(\rho_s - \rho_f)g(1 - \phi)/12h\eta\phi, \tag{11.25}$$

in which h is the height of the rock column through which the melt flows to its collection region. Equating this to the melt flux to the veinlets given by Eq. (11.24), the average width of the veinlets required to satisfy the stress assisted flux of melt from the regions between veins is

$$s = \sqrt[3]{32kh\phi\sigma_a/N(\rho_s - \rho_f)g(1 - \phi)a^2}. \tag{11.26}$$

Figure 11.18 shows graphically how the time required to extract 10 vol.% of melt from a protolith varies with temperature for different melt water contents

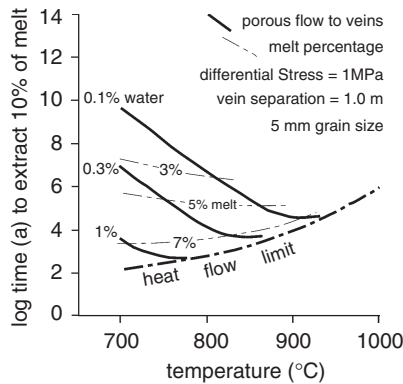


Fig. 11.18. Computed time (in years) to extract 10 vol.% of melt by shear-enhanced compaction from a hypothetical quartzofeldspathic protolith of grain diameter 5 mm, containing 0.1, 0.3, and 1.0 wt.% water. Melt is assumed to accumulate in veinlets, separated by 1 m, that inflate until they are sufficiently permeable to drain melt upwards by virtue of the density contrast between melt and solids. At short times, extraction rate is limited by heat flow. Applied differential stress is assumed to be 1 MPa. The long times required for dry melts combined with low temperatures can be reduced proportionally by increasing the differential stress and, hence, distortional strain rate. Contours are shown for melt fraction (percent). Melt viscosity is assumed to follow the Hess and Dingwell (1996) description. The combination of melt extraction by shear-enhanced compaction and gravity driven flow through veins allows even viscous melts to be extracted from their protoliths to form plutons in geologically realistic times.

at a constant differential stress of 1 MPa. The relationships between water content, temperature, melt viscosity, and melt fraction are as given by Eqs. (11.8), (11.9) and (11.10). The distortional part of the flow and the influence of local effective stress on permeability are neglected. Figure 11.19 shows graphically how veinlet thickness (Eq. (11.26)) varies for two cases: (1) where the rate of compaction retains the same value (10^{-13} s^{-1}) at all temperatures (in which case the stress decreases with temperature), and (2) where the applied stress retains the same value of 1 MPa at all temperatures. The range of vein thicknesses and separations predicted are reasonable when compared with the structure of migmatite complexes seen in the field (Chapter 10). The predicted time scales are also reasonable when compared to the expected duration of synorogenic magmatic cycles ($<10 \text{ Ma}$). A minimum time limit is imposed on the melt extraction process because it cannot run faster than the

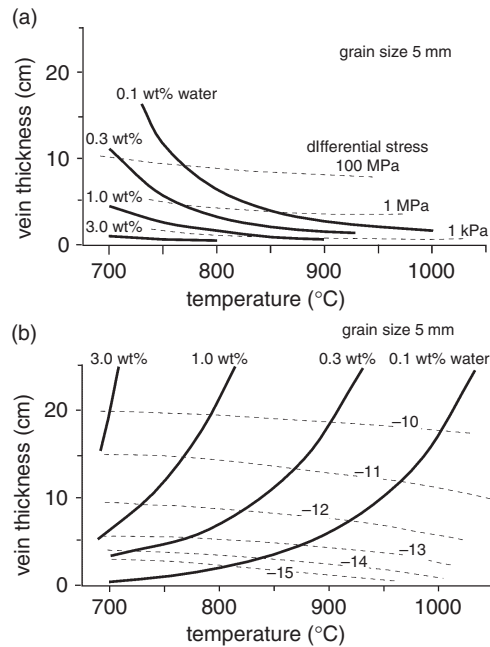


Fig. 11.19. Graphs showing the expected average thickness of veins in a vein network of average spacing 1 m in a protolith of mean grain size 5 mm for the water contents indicated, such that the rate of density driven flow through the veinlets equals the rate of supply of melt to the veins by shear-enhanced compaction. (a) is for a constant compaction rate of 10^{-13} s^{-1} , which corresponds to 10% volume loss from the protolith in 30 000 years. Contours of constant differential stress (dashed lines) are shown. (b) is for a constant applied differential stress of 1 MPa. Contours of constant log compressive strain rate (dashed lines) are shown.

rate at which heat is supplied for the melting reactions. It is also assumed that the dP/dT for the melting reaction will not lead to freezing on depressurization. Without the suggested two-stage melt separation process involving local non-hydrostatic stress gradients to push melt into veinlets, followed by gravitational separation in the veinlets, gravity driven porous flow as a separation mechanism would be slower by approximately the ratio of intergranular permeability to vein network permeability (i.e., about 10^5). This would require longer times than geologically available to separate melts of viscosities greater than about 10^6 Pa s.

11.5 Conclusions

The flow of partially molten rocks that gives rise to a granitic melt may involve granular flow, wherein solid crystals slide over one another. The accommodation process may be frictional with dilatation, or involve diffusive redistribution of material of the solid phases in the melt to bring about unlocking of asperities with lesser amounts of dilatation. Some fracturing of solid grains may also be produced. At relatively low temperatures, where the rock may be strong enough, flow of the matrix of solid grains may involve intracrystalline plasticity. The limited importance of the latter, deduced from the appearance of naturally deformed partially molten rocks and from modeling based on extrapolation of laboratory-determined constitutive flow laws, also tells us that partially molten granitic rocks must be extremely weak, able to flow at geological strain rates at differential stresses on the order of 1 MPa or less, according to the temperature. Vertical intervals in the lower crust that are partially molten must therefore be extremely effective tectonic detachment horizons.

The structure of natural partially molten rocks demonstrates that they are capable of being tectonically fractured or may develop cracks as a result of volume expansion on melting. Also, they may develop more “ductile” melt filled voids, such as interboudin partitions and vein networks, and shear zones. The latter may be effective at facilitating melt drainage by linking extensional fractures if granular flow involves substantial dilatancy. Experiments show that an increase in melt percentage causes dramatic weakening. Once the melt fraction in a shear zone becomes higher than the surroundings it would be expected to continue as a localized zone of weakness.

The density difference between melt and its protolith leads to a gravitational potential for the separation of melt by porous flow between grains. However, for viscous fluids such as granitic melts, homogeneous intergranular porous flow is too slow to cause segregation of granitic liquids over geologically

reasonable periods of time. Provided *local* differential stress gradients may develop between veinlets and adjacent volumes of partially molten protolith, pore fluid pressure gradients may be induced that are hundreds to thousands of times greater than the gravitational potential gradient, and able to drive melt transport from intergranular spaces to the much more permeable vein network. Gravity driven drainage of the vein network then may separate the melt in a geologically reasonable time scale.

11.6 Acknowledgements

This work was supported by UK NERC grants GR9/2640 and GR3/13062. Experimental work was aided by experimental officer Robert Holloway. Ben Holtzman is thanked for providing Fig. 11.14b. Helpful and constructive reviews by Gayle Gleason and an anonymous reviewer led to considerable improvements to this chapter.

References

- Arzi, A. A. (1978). Critical phenomena in the rheology of partially melted rocks. *Tectonophysics*, **44**, 173–84.
- Auer, F., Berkhemer, H. and Oehlschlegel, G. (1981). Steady-state creep of fine grain granite at partial melting. *Journal of Geophysics*, **49**, 89–92.
- Bourbie, T. and Zinzner, B. (1985). Hydraulic and acoustic properties as a function of porosity in Fontainebleau sandstone. *Journal of Geophysical Research*, **90**, 11 524–32.
- Brace, W. F. and Martin, R. J. (1968). A test of the law of effective stress for crystalline rocks of low porosity. *International Journal of Rock Mechanics and Mining Sciences*, **5**, 415–26.
- Brown, M., Averkin, Y. A., McLellan, E. L. and Sawyer, E. W. (1995). Melt segregation in migmatites. *Journal of Geophysical Research*, **100**, 15 665–79.
- Brown, M. A., Brown, M., Carlson, W. D. and Denison, C. (1999). Topology of melt-flow networks in the deep crust: inferences from three-dimensional images of leucosome geometry in migmatites. *American Mineralogist*, **84**, 1793–818.
- Bruhn, D., Groebner, N. and Kohlstedt, D. L. (2000). An interconnected network of core-forming melts produced by shear deformation. *Nature*, **403**, 883–6.
- Bussod, G. Y. and Christie, J. M. (1991). Textural development and melt topology in spinel lherzolite experimentally deformed at hypersolidus conditions. *Journal of Petrology*, **32**, 17–39.
- Chekmir, A. S. & Epel'baum, M. B. (1991). Diffusion in magmatic melts: new study. In *Physical Chemistry of Magmas*, ed. L. L. Perchuk and I. Kushiro. *Advances in Physical Geochemistry*, 9, New York: Springer-Verlag, pp. 99–119.
- Clarke, D. R. (1987). On the equilibrium thickness of intergranular glass phases in ceramic materials. *Journal of the American Ceramic Society*, **70**, 15–22.
- Clemens, J. D. and Vielzeuf, D. (1987). Constraints on melting and magma production in the crust. *Earth and Planetary Science Letters*, **86**, 287–306.

- Curran, J. H. and Carroll, M. M. (1979). Shear stress enhancement of void compaction. *Journal of Geophysical Research*, **84**, 1105–12.
- Daines, M. and Kohlstedt, D. L. (1997). Influence of deformation on melt topology in peridotites. *Journal of Geophysical Research*, **107**, 10 257–71.
- Dell'Angelo, L. N. and Tullis, J. (1988). Experimental deformation of partially melted granitic aggregates. *Journal of Metamorphic Geology*, **6**, 495–516.
- Dell'Angelo, L. N., Tullis, J. and Yund, R. A. (1987). Transition from dislocation creep to melt-enhanced diffusion creep in fine-grained granitic aggregates. *Tectonophysics*, **139**, 325–32.
- Dimanov, A., Dresen, G. and Wirth, R. (1998). High-temperature creep of partially molten plagioclase aggregates. *Journal of Geophysical Research*, **103**, 9651–64.
- D'Lemos, R. S., Brown, M. and Strachan, R. A. (1992). The relationship between granite and shear zones: magma generation, ascent and emplacement in a transpressional orogen. *Journal of the Geological Society London*, **149**, 487–90.
- Drury, M. R. and Fitzgerald, J. D. (1996). Grain boundary melt films in experimentally deformed olivine-orthopyroxene rock; implications for melt distributions in upper mantle rocks. *Geophysical Research Letters*, **23**, 701–4.
- Gapais, D. and Barbarin, B. (1986). Quartz fabric transition in a cooling syntectonic granite (Hermitage, France). *Tectonophysics*, **25**, 357–70.
- Gleason, G. C., Bruce, V. and Green, H. W. (1999). Experimental investigation of melt topology in partially molten quartzo-feldspathic aggregates under hydrostatic and non-hydrostatic stress. *Journal of Metamorphic Geology*, **17**, 705–22.
- Green, H. W. & Borch, R. S. (1990). High pressure and temperature deformation experiments in a liquid confining medium. In *The Brittle-Ductile Transition in Rocks*, ed. A. G. Duba, W. B. Durham, J. W. Handin and H. F. Wang. Geophysical Monograph 56, American Geophysical Union, pp. 195–200.
- Hess, P. C. (1994). Thermodynamics of thin films. *Journal of Geophysical Research*, **99**, 7219–29.
- Hess, K.-U. and Dingwell, D. B. (1996). Viscosities of hydrous leucogranite melts: a non Arrhenian model. *American Mineralogist*, **81**, 1297–300.
- Hiraga, T., Anderson, I. M., Zimmerman, M. E., Mei, S. and Kohlstedt, D. L. (2002). Structure and chemistry of grain boundaries in deformed olivine + basalt and partially molten lherzolite aggregates: evidence of melt-free grain boundaries. *Contributions to Mineralogy and Petrology*, **144**, 163–75.
- Hirth, G. and Kohlstedt, D. L. (1995a). Experimental constraints on the dynamics of the partially molten upper mantle: deformation in the diffusion creep regime. *Journal of Geophysical Research*, **100**, 1981–2001.
- Hirth, G. and Kohlstedt, D. L. (1995b). Experimental constraints on the dynamics of the partially molten upper mantle: deformation in the dislocation creep regime. *Journal of Geophysical Research*, **100**, 15 441–9.
- Holtzman, B. K., Groebner, N. J., Zimmerman, M. E., Ginsberg, S. B. and Kohlstedt, D. L. (2003a). Stress-driven melt segregation in partially molten rocks. *Geochemistry, Geophysics, Geosystems*, **4**, 8607, doi:10.1029/2001GC000258.
- Holtzman, B. K., Kohlstedt, D. L., Zimmerman, M. E., Heidelbach, F., Hiraga, T. and Hustoft, J. (2003b). Melt segregation and strain partitioning: implications for seismic anisotropy and mantle flow. *Science*, **301**, 1227–30.
- Jeffrey, D. J. and Acrivos, A. (1976). The rheological properties of suspensions of rigid particles. *Journal of the American Institute of Chemical Engineers*, **22**, 417–32.
- Jin, Z. -M., Green, H. W. and Zhou, Y. (1994). Melt topology during dynamic partial melting of mantle peridotite. *Nature*, **372**, 164–7.

- Laporte, D. (1994). Wetting behavior of partial melts during crustal anatexis: the distribution of hydrous silicic melts in polycrystalline aggregates of quartz. *Contributions to Mineralogy and Petrology*, **116**, 486–99.
- Lejeune, A.-M. and Richet, P. (1995). Rheology of crystal-bearing silicate melts: an experimental study at high viscosities. *Journal of Geophysical Research*, **100**, 4215–29.
- Luan, F.-C. and Paterson, M. S. (1992). Preparation and deformation of synthetic aggregates of quartz. *Journal of Geophysical Research*, **97**, 301–20.
- Marchildon, N. and Brown, M. (2002). Grain-scale melt distributions in two contact aureole rocks: implication for controls on melt localization and deformation. *Journal of Metamorphic Geology*, **20**, 381–96.
- Mecklenburgh, J. and Rutter, E. H. (2003). On the rheology of partially molten synthetic granite. *Journal of Structural Geology*, **25**, 1575–85.
- McKenzie, D. (1984). The generation and compaction of partially molten rock. *Journal of Petrology*, **25**, 713–65.
- McKenzie, D. (1985). The extraction of magma from the crust and mantle. *Earth and Planetary Science Letters*, **74**, 81–91.
- Mortensen, A. (1997). Kinetics of densification by solution-precipitation. *Acta Materialia*, **2**, 749–58.
- Muir Wood, D. (1990). *Soil Behaviour and Critical State Soil Mechanics*. New York: Cambridge University Press.
- Nicolas, A. and Ildefonse, B. (1996). Flow mechanism and viscosity in basaltic magma chambers. *Geophysical Research Letters*, **23**, 2013–16.
- Paquet, J. and François, P. (1980). Experimental deformation of partially melted granitic rocks at 600° to 900°C and 250 MPa confining pressure. *Tectonophysics*, **68**, 131–46.
- Paquet, J., François, P. and Nedelec, A. (1981). Effect of partial melting on rock deformation: experimental and natural evidences for rocks of granitic compositions. *Tectonophysics*, **78**, 545–65.
- Park, Y. & Means, W. D. (1996). Crystal rotation and growth during grain flow in a deforming crystal mush. In *Evolution of Geological Structures in Micro- to Macro-Scales*, ed. S. Sengupta. London: Chapman and Hall, pp. 245–58.
- Paterson, M. S. (1990). Rock deformation experimentation. In *The Brittle–ductile Transition in Rocks*, ed. A. G. Duba, W. B. Durham, J. W. Handin and H. F. Wang. American Geophysical Union Geophysical Monograph 56, pp. 187–94.
- Paterson, M. S. (1995). A theory for granular flow accommodated by material transfer via an intergranular fluid. *Tectonophysics*, **245**, 135–52.
- Paterson, M. S. (2001). A granular flow theory for the deformation of partially molten rock. *Tectonophysics*, **335**, 51–61.
- Paterson, M. S. & Luan, F.-C. (1990). Quartzite rheology under geological conditions. In *Deformation Mechanisms, Rheology and Tectonics*, ed. R. J. Knipe and E. H. Rutter. Geological Society of London Special Publication 54, pp. 299–308.
- Persikov, E. S., Bukhtiyarov, P. G. and Polskoy, S. F. (1990). The effects of volatiles on the properties of magmatic melts. *European Journal of Mineralogy*, **2**, 621–42.
- Renner, J., Evans, B. and Hirth, G. (2000). On the rheologically critical melt percentage. *Earth and Planetary Science Letters*, **181**, 585–94.
- Renner, J., Viskupic, K., Hirth, G. and Evans, B. (2003). Melt extraction from partially molten peridotites. *Geochemistry, Geophysics, Geosystems*, **4**, 8606, doi:10.1029/2002GC000369.

- Roscoe, R. (1952). The viscosity of suspensions of rigid spheres. *British Journal of Applied Physics*, **3**, 267–9.
- Rosenberg, C. L. (2001). Deformation of partially molten granite: a review and comparison of experimental and natural case studies. *International Journal of Earth Sciences (Geologisches Rundschau)*, **90**, 60–76.
- Rosenberg, C. L. and Handy, M. R. (2000). Syntectonic melt pathways during simple shearing of a partially molten rock analogue (norcamphor-benzamide). *Journal of Geophysical Research*, **105**, 3135–49.
- Rosenberg, C. L. and Handy, M. R. (2002). Mechanisms and orientation of melt segregation paths during pure shearing of a partially molten rock analog (norcamphor-benzamide). *Journal of Structural Geology*, **23**, 1917–32.
- Rosenberg, C. L. and Riller, U. (2000). Partial melt topology in statically and dynamically recrystallized granite. *Geology*, **28**, 7–10.
- Rutter, E. H. (1972). Effects of strain rate changes on the strength and ductility of Solnhofen limestone at low temperature and confining pressures. *International Journal of Rock Mechanics and Mining Sciences*, **9**, 183–9.
- Rutter, E. H., (1997). The influence of deformation on the extraction of crustal melts: a consideration of the role of melt-assisted granular flow. In *Enhanced Fluid Transport in the Earth's Crust*, ed. M. B. Holness. Deformation. London: Chapman and Hall, pp. 82–110.
- Rutter, E. H. and Neumann, D. H. K. (1995). Experimental deformation of partially molten Westerly granite, with implications for the extraction of granitic magmas. *Journal of Geophysical Research*, **100**, 15 697–715.
- Sawyer, E. W. (2001). Melt segregation in the continental crust: distribution and movement of melt in anatectic rocks. *Journal of Metamorphic Geology*, **19**, 291–310.
- Skempton, A. W. (1954). The pore pressure coefficients A and B. *Géotechnique*, **4**, 143–7.
- Smith, G. N. (1990). *Elements of Soil Mechanics*. Oxford: Blackwell.
- Snoke, A. W., Kalakay, T. J., Quick, J. E. and Sinigoi, S. (1999). Development of a deep crustal shear zone in response to tectonic intrusion of mafic magma into the lower crust, Ivrea–Verbano zone, Italy. *Earth and Planetary Science Letters*, **166**, 31–45.
- Tullis, T. E. & Tullis, J. (1986). Experimental rock deformation techniques. In *Mineral and Rock Deformation: Laboratory Studies* ed. B. E. Hobbs and H. C. Heard. Geophysical Monograph 36, American Geophysical Union, pp. 297–324.
- van der Molen, I. and Paterson, M. S. (1979). Experimental deformation of partially melted granite. *Contributions to Mineralogy and Petrology*, **70**, 299–318.
- Vigneresse, J. L. (1995). Control of granite emplacement by regional deformation. *Tectonophysics*, **249**, 173–86.
- Viskupic, K. M., Renner, J., Hirth, G. and Evans, B. (2001). Melt segregation from partially molten peridotites. *EOS, Transactions of the American Geophysical Union*, **82**, F1107–F8.
- Waff, H. S. and Faul, U. H. (1992). Effects of crystalline anisotropy on fluid distribution in ultramafic partial melts. *Journal of Geophysical Research*, **97**, 9003–14.
- Wen, S. and Nekvasil, H. (1994). Ideal associated solutions: application to the system albite-quartz-H₂O. *American Mineralogist*, **79**, 316–31.
- Wickham, S. M. (1987). The segregation and emplacement of granitic magmas. *Journal of the Geological Society London*, **144**, 281–97.

Zimmerman, M. E., Zhang, S., Kohlstedt, D. L. and Karato, S. (1999). Melt distribution in mantle rocks deformed in shear. *Geophysical Research Letters*, **26**, 1505–8.

List of Symbols Used

σ_i	Principal stress component (Pa), $i = 1, 2,$ or 3 .
ϵ_j	Conventional strain component, $j = 1, 2,$ or 3 .
ρ	Pore fluid (melt) pressure (Pa).
A, B	Skempton pore pressure coefficients.
x, z	Distance along coordinate axis (m).
η	Melt viscosity (Pa s).
k	Matrix permeability (m^2).
ϕ	Porosity (= melt fraction).
θ	Dihedral angle (degrees).
δ_c	Compaction distance (m).
w_0	Melt velocity (m s^{-1}).
τ_0	Compaction time (s).
h	Layer thickness and height of rock column (m).
μ	Effective viscosity of solid matrix (Pa s).
ρ_s	Solid density (kg m^{-3}).
ρ_f	Melt density (kg m^{-3}).
γ_{sm}	Melt–solid surface energy (J m^{-2}).
γ_{ss}	Solid–solid surface energy (J m^{-2}).
κ	Pore pressure multiplier in effective stress law.
s	Vein width (m).
N	Number of veins per meter (m^{-1}).
$2a$	Distance between veins (m).
R	Gas constant ($\text{J K}^{-1} \text{mol}^{-1}$).
T	Temperature (K).
T_C	Temperature ($^{\circ}\text{C}$).
Ψ	Water content of melt (wt.%).
∇^2	Laplacian operator.
H	Activation enthalpy (J mol^{-1}).
d	Grain diameter (m).
g	Gravitational acceleration (ms^{-2}).
D	Diffusion coefficient ($\text{m}^2 \text{s}^{-1}$).
V	Solid phase molar volume (m^3).
U	Melt flow velocity (m s^{-1}).
c'	Equilibrium molar concentration.
n	Stress exponent in flow law.
r	Melt fraction exponent.
q	Exponent in Einstein–Roscoe equation.
a, b, c	Coefficients in Hess–Dingwell viscosity formula.
C_i, C'_i	Empirical constants in flow laws, $i = 1, 2,$ or 3 .